TIME-FREQUENCY ANALYSIS OF SOMATOSENSORY POTENTIALS EVOKED BY VIBROTACTILE STIMULATION OF THE FINGERTIP

by

Kutluhan MAHMAT

B.S., Biomedical Engineering, Kocaeli University, 2018

Submitted to the Institute of Biomedical Engineering
in partial fulfillment of the requirements
for the degree of
Master of Science
in
Biomedical Engineering

Boğaziçi University
2022

ACKNOWLEDGMENTS

I would like to express my gratitude to everyone that contributed to my thesis; first and foremost, express my sincere gratitude to Prof. Dr. Burak Güçlü and Assoc. Prof. Dr. Mustafa Zahid Yıldız for their continuous assistance and valuable contributions while deciding the MSc thesis topic, analysis of the data and writing my thesis document.

I would, also, like to express my thanks to lab mates in Tactile Research Laboratory; Begüm Devlet Kılıçkap, Enes Tarık Aras, and İsmail Erbaş.

Last but not the least, I would like to express my sincere appreciation to my family for their endless support.

ACADEMIC ETHICS AND INTEGRITY STATEMENT

I, Kutluhan MAHMAT, hereby certify that I am aware of the Academic Ethics and Integrity Policy issued by the Council of Higher Education (YÖK) and I fully acknowledge all the consequences due to its violation by plagiarism or any other way.

Name :

Signature:

Date:

ABSTRACT

TIME-FREQUENCY ANALYSIS OF SOMATOSENSORY POTENTIALS EVOKED BY VIBROTACTILE STIMULATION OF THE FINGERTIP

Tactile sensory feedback has become an essential topic for neural engineering to model advanced neuroprostheses providing artificial sensations. For this purpose, it is required to understand human brain activity related to some parameters (e.g., sensation level, frequency, time window, etc.) of tactile somatosensory inputs. There have been numerous studies related to tactile psychophysical channels and their properties. However, so far, a link could not be established between psychophysical data and somatosensory evoked potentials (SEPs) generated by vibrotactile stimulation in humans. Therefore, the fundamental goal of this study is to analyze SEPs, which were generated by 40 Hz vibrotactile stimulus applied to human fingertip, over the S1 cortex. EEG data were collected and analyzed in a previous study by Yildiz (2013), but it was reanalyzed by different methods in this thesis. In particular, seven healthy adult subjects participated in psychophysical experiments. EEG recordings were obtained for several (NS, 10dB, 20dB, and 30dB) sensation levels (SLs) at and above threshold. They were collected at the forehead and Cpi-Cpc as mechanically evoked SEPs by gold surface EEG electrodes on the human scalp over the S1 cortex. The data were analyzed by Continuous Wavelet Transform (CWT) by means of Morse Wavelet at different time windows of stimulation. Consequently, no significant differences were found in frequency band energies for different sensation levels except some combinations in the low gamma band at the stimulus onset. Given the small sample size, these results imply that non-invasive EEG recording methods may not be adequate to measure fine psychophysical parameters in this study for flutter sensation at 40 Hz.

Keywords: tactile sensory feedback, tactile psychophysical channels, primary somatosensory cortex, somatosensory evoked potentials, morse wavelet, continuous wavelet transform.

ÖZET

PARMAK UCUNUN MEKANİK TİTREŞİMLE UYARILMASIYLA OLUŞAN BEDEN DUYUSU POTANSİYELLERİNİN ZAMAN-FREKANS ANALİZİ

Dokunsal duyu geribeslemesi, yapay hisler sağlayan gelişmiş nöroprotezler modellemek amacıyla nöromühendislik açısından önemli bir konu haline gelmiştir. Bu amaçla beyin aktivitesinin mekanik titreşimsel uyaranların duyu seviyesi, frekans, zaman penceresi gibi bazı parametreleriyle arasındaki ilişkisini anlamak önemlidir. Psikofiziksel vibrotaktil kanallar ve özellikleriyle ilişkili literatürde çok çalışma bulunmaktadır. Ancak, şimdiye kadar psikofiziksel veriler ve titreşimli dokunsal girdilere karşı üretilen beden duyusu korteksindeki uyarılmış potansiyeller arasında bir bağlantı kurulamamıştır. Bu çalışmanın amacı insan parmak ucunda 40 Hz titreşimli dokunsal uyaranla oluşan beden duyusu potansiyellerinin korteks üzerindeki kafa derisinden ölçümünü analiz etmektir. Elektroensefalogram (EEG) kayıtları Yildiz (2013) tarafından önceki bir insan çalışmasında toplanmış ve analiz edilmiştir. Ancak, bu tezde farklı yöntemler kullanılarak yeniden analiz edilmişlerdir. Yedi yetişkin ve sağlıklı katılımcı psikofizik deneylerine katılmıştır. EEG kayıtları eşik ve eşik üzeri birçok farklı duyu seviyesi (NS, SL10, SL20 ve SL30 dB) için toplanmıştır. Kayıtlar, mekanik uyarana ilişkin beden duyusu potansiyelleri olarak alın bölgesinden ve Cpi-Cpc montajıyla birincil beden duyusu korteksi üzerindeki kafa derisinden altın yüzeyli elektrotlar kullanılarak alınmıştır. Veriler, Morse dalgacık dönüşümüyle uyaranın farklı zaman pencereleri için analiz edilmiştir. Farklı duyu seviyeleri için low gamma bandının bazı kombinasyonları haricinde frekans bant enerjilerinde belirgin farklılıklar bulunamamıştır. Katılımcı sayısına göre bu sonuçlar, girişimsel olmayan EEG kayıt yöntemlerinin 40 Hz uyaran için hassas psikofiziksel parametreleri ölçmede yeterli olmadığını göstermektedir.

Anahtar Sözcükler: dokunsal duyu geribeslemesi, psikofiziksel taktil kanallar, birincil bedenduyusu korteksi, beden duyusu korteksindeki uyarılmış potansiyeller, morse dalgacıkları, sürekli dalgacık dönüşümü.

TABLE OF CONTENTS

LIST OF FIGURES

LIST OF TABLES

LIST OF SYMBOLS

$\Psi_{P,\gamma}(\omega)$	Fourier transform
$U(\omega)$	Unit step function
$\alpha_{P,\gamma}$	Normalizing constant
P^2	Time-bandwidth product
γ	Symmetry of Morse Wavelet
β	Time domain decay
$(\frac{P^2}{\gamma})^{\frac{1}{\gamma}}$	Peak frequency

LIST OF ABBREVIATIONS

BMI	Brain machine interface
RA1	Rapidly Adapting Type 1
RA2	Rapidly Adapting Type 2
SA1	Slowly Adapting Type 1
SA2	Slowly Adapting Type 2
CNS	Central Nervous System
P	Pacinian
NP	Non-Pacinian
PC	Pacinian Channel
S1	Primary Somatosensory Cortex
S2	Secondary Somatosensory Cortex
EP	Evoked Potential
AEP	Auditory Evoked Potential
VEP	Visual Evoked Potential
SEP	Somatosensory Evoked Potential
SL	Sensation Level
NS	No stimulus
EEG	Electroencephalography
MEG	Magnetoencephalography
ECoG	Electrocorticography
SP	Signal Processing
LP	Lowpass
HP	Highpass
BP	Bandpass
FT	Fourier Transform
FFT	Fast Fourier Transform
WT	Wavelet Transform
DWT	Discrete Wavelet Transform

WAVEDEC	Wavelet Decomposition
MODWT	Maximal Overlap Discrete Wavelet Transform
CWT	Continuous Wavelet Transform
TW	Time Window
TFA	Time-Frequency Analysis

1. INTRODUCTION

The somatosensory system is an essential part of the human nervous system, which allows an individual to perceive body awareness, touch, pain, and temperature change [1, 2, 3]. By means of the ability of tactile fibers to transmit neural information, a human can successfully distinguish textures such as smoothness and shape of objects and grip of them. Fundamentally, the skin is separated into three subcategories which are hairless, or with another name glabrous, hairy skin and mucocutaneous skin, and human glabrous skin has four kinds of mechanoreceptors that are Meissner corpuscles, Merkel cells, Ruffini endings, and Pacinian corpuscles [4, 5, 6]. They have unique characteristics which have a capability to response under mechanical deviations or forces, and they vary spike responses based on the size of the receptive field, pressure, and frequency parameters of the stimulus [7].

In the human body, there are many sensory systems, and tactile system is the one that can involve our ability to sense vibration, stretch, and pressure [1]. These characteristic features of tactile perception may readily be analyzed by electrophysiological or psychophysical methods. Stimulations, among them, can be either electrical or mechanical, and although former of which can be favored in clinical studies because of simplicity and higher responses, the latter one was preferred in this study since mechanical vibrations are more relevant in nature.

The main goal of this study is to compare somatosensory potentials evoked by the vibrotactile stimulus of the fingertip and related to psychophysical SLs. Hypothetically, it has been expected that stimulus amplitude close to threshold level has an influence on evoked potential parameters such as frequency band and time windows. Experiments and analyses were conducted by Yildiz (2013), but significant results could not be found for vibrotactile stimulus within a certain parameter set [8]. Therefore, the time-frequency analysis method was performed to reanalyze the same data in this thesis. However, in the results, any correlation could not be observed. Hence, non-invasive

EEG recordings may have a limited contribution to understanding the effects of tactile sensory feedback in brain-machine interfaces (BMIs) and neuroprosthesis. However, invasive electrocorticography (ECoG) may be more useful for that purpose.

2. BACKGROUND

2.1 Sense of Touch by Glabrous Skin

Sense of touch is a sort of connection between object and human hand, and it has, basically, two types: active touch and passive touch, the former of which is associated with the conscious orientation of the skin using a receiver such as holding or lifting of a glass. On the contrary, various outside factors are needed for passive touch [9]. Thanks to its compliable and soft features, the skin of humans is involved in the sense of touch when they touch a tool [10, 1]. Skin is a multi-layered and biggest organ for humans, and it facilitates tactile sensation. There are, fundamentally, three types of skin that are glabrous, hairy, and mucocutaneous skin [7].

2.1.1 Mechanoreceptors in the Glabrous Skin

The glabrous skin, among those, is generally found on our soles and palms, and it has 4 mechanoreceptors: Ruffini endings, Pacinian corpuscles, Merkel cells, and Meissner corpuscles. Those differ from each other, corresponding to deepness, surface morphology, and pattern of innervation. In terms of response properties, they are called either rapidly (RA) or slowly adapting (SA) fibers. While the RA fibers stop responding within a very short time if the stimulus is stationary, the SA fibers can respond when they are aroused from skin indentation, which is steady [1].

Hence, the sense of touch in glabrous skin is mediated by 4 afferent fibers that are slowly adapting to type 1 (SA1), slowly adapting type 2 (SA2), rapidly adapting type 1 (RA1), and rapidly adapting type 2 (RA2) [5]. Among these fibers, SA1 refers to Merkel disc-receptor-fibers, SA2 points out Ruffini endings, RA1 represents Meissner fibers, and RA2 indicates Pacinian corpuscles, or PC, fibers. While Ruffini and Pacinian corpuscles stay within the dermis that is cover 1-4 mm thickness, Merkel cells, and

Meissner corpuscles is found within the epidermis (comprise between 0.07-0.12 mm thickness) (Figure 2.1) [11, 12].

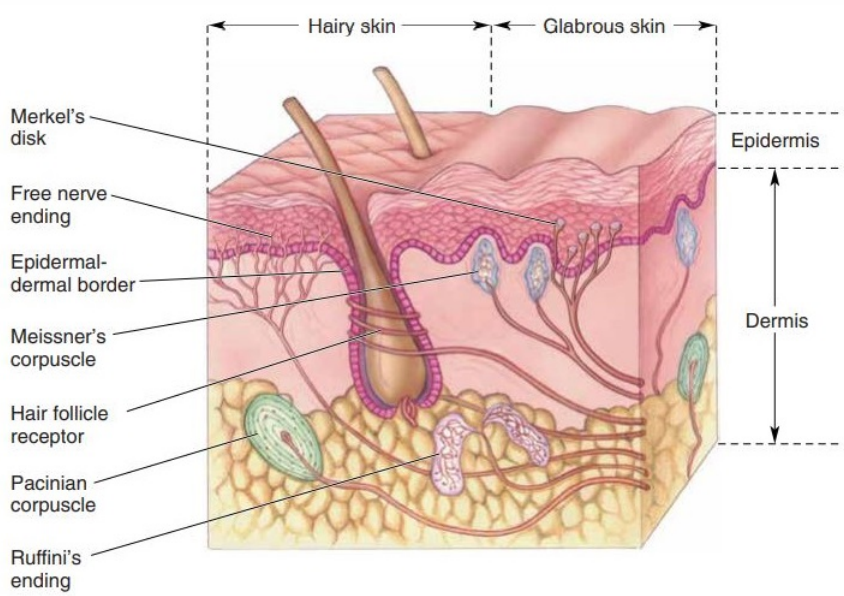

Figure 2.1 Mechanoreceptors in the human glabrous skin [11]

2.1.2 Receptive Fields in the Glabrous Skin

In addition to adaptation properties, these mechanoreceptors differ from each other in terms of their spatial sensitivity. The spatial sensitivity is varied depending on the receptive field, and the receptive field is a small skin area that tactile information is transmitted by any type of mechanoreceptors. Figure 2.2 shows the receptive field areas of the mechanoreceptors in the human hand shown by Johansson and Valbo [13]. According to Figure 2.2, blue and red spots represent tactile acuity, the contours exhibit sensitivity, and arrows monitor the skin stretch of each receptive field. For the contour map, sensitivity increases from a pink color to a red one. In the figure, mechanoreceptors which are located superficial levels (SA1 and RA1), have more tactile acuity compared to deeper layers (SA2 and RA2) of the human glabrous skin since, as it can be seen on the contour maps, their receptive fields have more red areas which represent high sensitivity. The capability to tactile acuity allows them to recognize

gaps, grates, and letter identification such as the Braille alphabet. On the other hand, although RA2 fibers (P channels) have only one red spot, its wide spot area provides maximum sensitivity to touch than superficial ones. This ability gives them to extract the tactile information from a larger area [1].

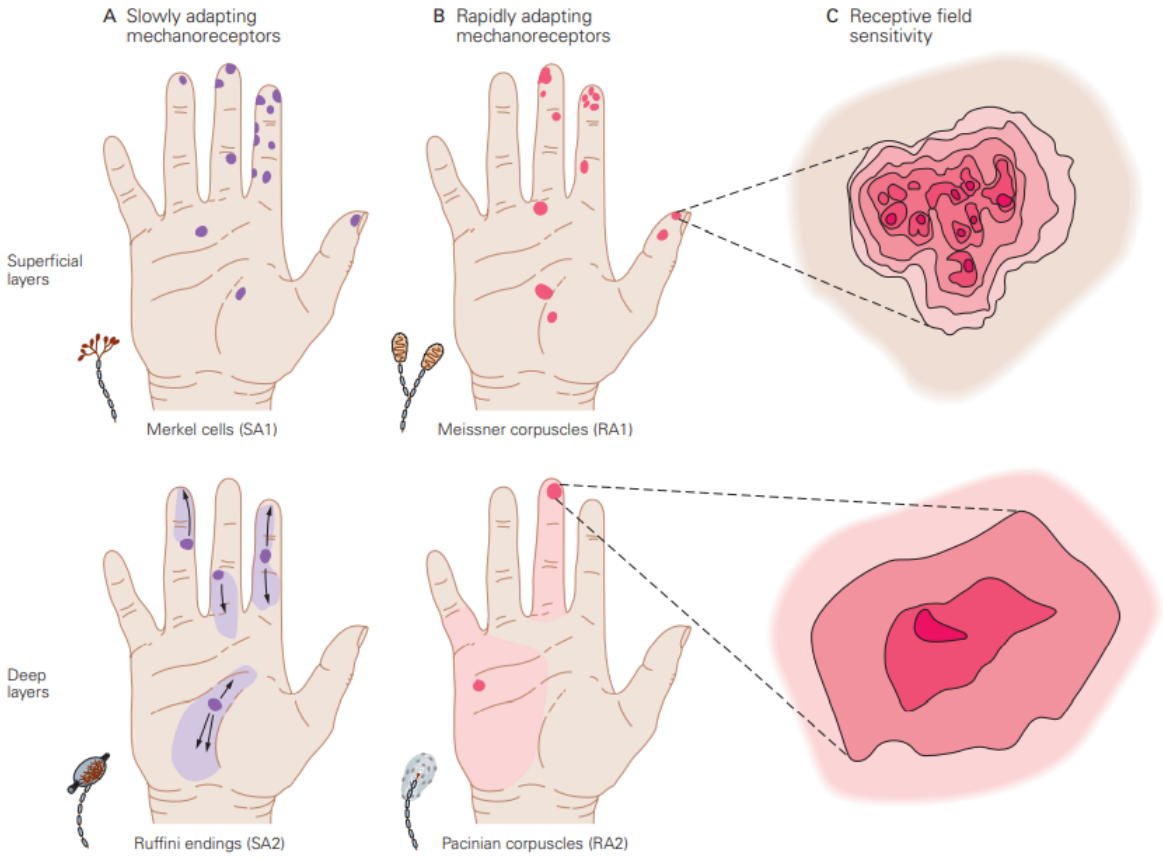

Figure 2.2 The receptive fields in the human glabrous skin [1].

In the literature, it has been proved that there is a robust mathematical connection between psychophysics and physiological parameters when it comes to the RA fibers so that behavior of psychophysics can be modeled by the activity of the neurons [14, 15, 16, 1, 17, 18]. Figure 2.3 displays the relationship between receptive field sizes and adaptation of the mechanoreceptive fibers. According to Figure 2.3, while RA fibers generate spikes at the onset and offset of the stimulus, SA fibers may sustain their responses whole stimulus duration [4].

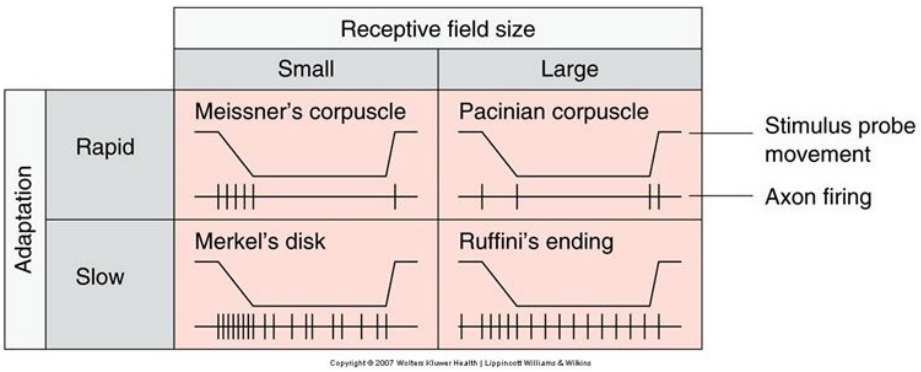

Figure 2.3 Influence of receptive field size and adaptation on the axon firing of the stimulus evoked by stimulus [4].

2.1.3 Sense of Vibration for Mechanoreceptive Fibers

The sensation of created oscillation of a tool closely located to the human glabrous skin is called a sense of vibration. In neuroscience, vibration motors, high-intensity focused ultrasound, musical instruments, or other types of sources can be used as tactile stimuli thanks to their pressure effect characteristics.

For mechanoreceptive fibers, except for their sensitivity and adaptation properties, their thresholds diverge from each other with respect to frequency. That is to say, every mechanoreceptive fiber class is more responsive in a certain frequency range. For instance, while slowly adaptive fibers produce a high amount of spike firing at a low frequency of stimulus, rapidly adaptive fibers have a tendency to evoke such firings at high frequencies.

In Figure 2.4, tactile threshold levels of humans and frequency characteristics of three mechanoreceptive fibers can be observed. According to the figure, it can be argued that each mechanoreceptive fibers act as a bandpass filter since every one of them has a different responsivity range in terms of frequency. For instance, while two of them (Merkel disks and Meissner corpuscles) have the higher ability in responsivity at lower frequency points, Pacinian corpuscles are good at responding to high-frequency levels. This is mainly because the lowest threshold level for a mechanoreceptive fiber at

a specific frequency means higher detection capability and responsivity at that point. Particularly, the stimulus frequency that is between 0.3-2 Hz, Merkel disks are more responsive. Another mechanoreceptor, Meissner corpuscles, has the lowest thresholds between 2-30 Hz frequency stimulus [19]. The Pacinian corpuscles are more responsive if only they are exposed to a high-frequency stimulus (30-500 Hz) [19, 20].

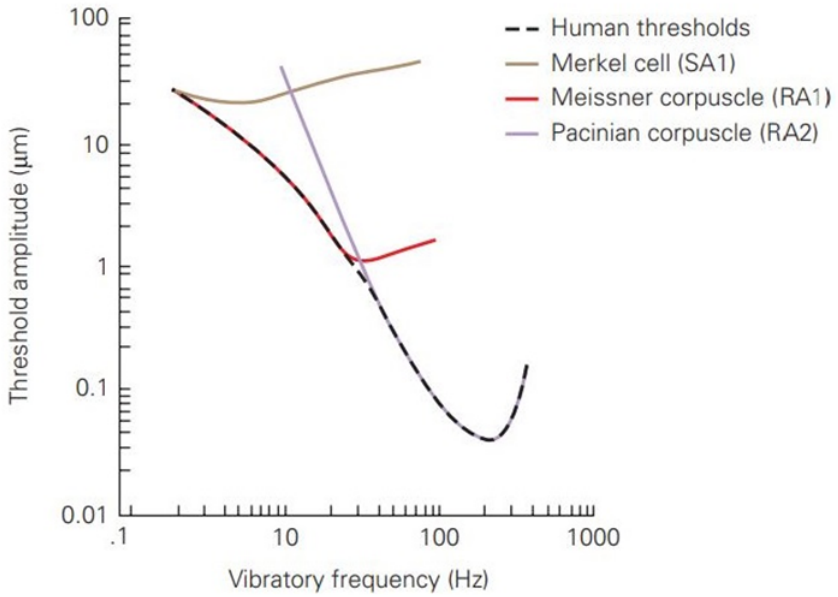

Figure 2.4 Neural thresholds of an individual and three mechanoreceptors [1, 11].

2.2 The Somatosensory System and its Central Pathways

2.2.1 Transduction of the Stimulus

Stimulus transduction is, or mechanoelectrical transduction, a transformation mechanism that transforms mechanical stimulus exposed by the skin into electro-chemical activities received and progressed by the human nervous system [13]. This mechanism has the same characteristic features for all mechanoreceptor types. Simple Pacinian corpuscle, sinusoidal vibration and human finger illustration can be seen in Figure 2.5. In Figure 2.5, connective tissue laminae have the fluid-filled structure of RA2 fibers that covers the tip of the Pacinian corpuscles [1, 11]. When mechanical forces are applied to the fingertip, the axon of the corpuscle transduces mechanical

information into electrical information. Then, the generated spike travels around the myelinated axon in order to convey the sensory information to the central nervous system (CNS) [11].

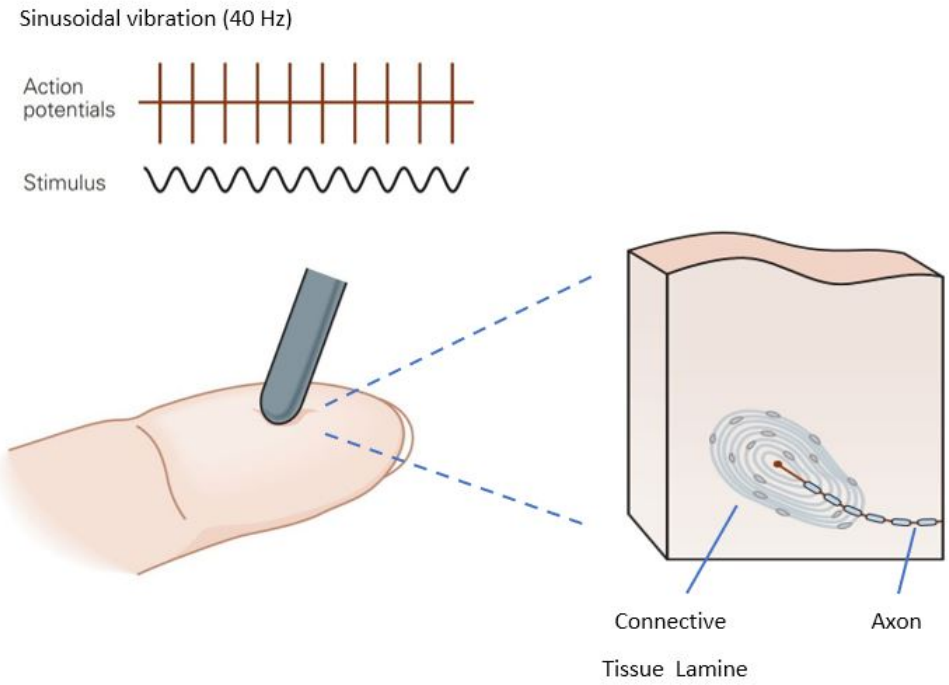

Figure 2.5 Simple illustration of Pacinian corpuscle [1].

2.2.2 Mechanosensitive Ion Channels

The chemical phenomenon begins with mechanosensitive ion channels. Both decreasing and increasing of the opening of the channels and gate changes have occurred if there is an applied force. Particularly, This applied force can be either directly or indirectly. It means that the concept can be revealed by either the interconnections between cytoskeletal components of intracellular or proteins of extracellular matrix and the ion channels or the membrane. [11]. Figure 2.6a shows that when the ion channels are induced directly by the increased membrane tension, the permeability of the membrane is increased, which results in depolarization of the membrane and transformation Na^{+} and Ca^{2+} from outside to inside the cell. In Figure 2.6b, the gate

is opened by an extracellular protein outside the cell. Furthermore, in Figure 2.6c, the same phenomenon is revealed by a cytoskeletal component inside the cell.

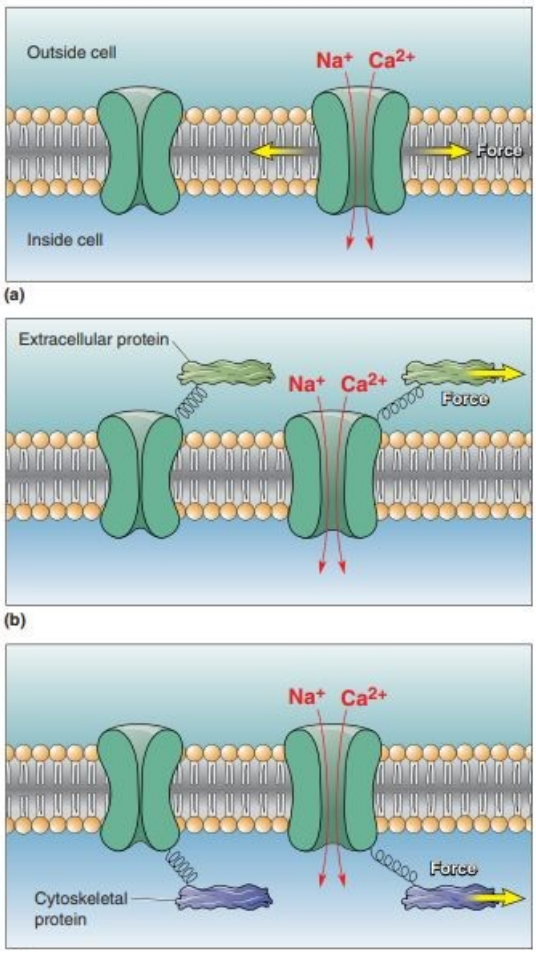

Figure 2.6 Mechanosensitive ion channels [11].

2.2.3 Primary Afferent Neurons

For the somatosensory system, the primary afferent neuron is a sort of neuron which carries sensory information from the receptors of the somatosensory system to the brain stem and spinal cord. As it can be seen in Figure 2.7, there is an interconnection between the spinal cord and primary afferent neurons, and it is called as dorsal root. The body of the dorsal root extends throughout ganglion cells of the dorsal root. It has two branches, ones goes to the spinal cord segment and the other ascends the dorsal column nucleus for further processing [1, 11].

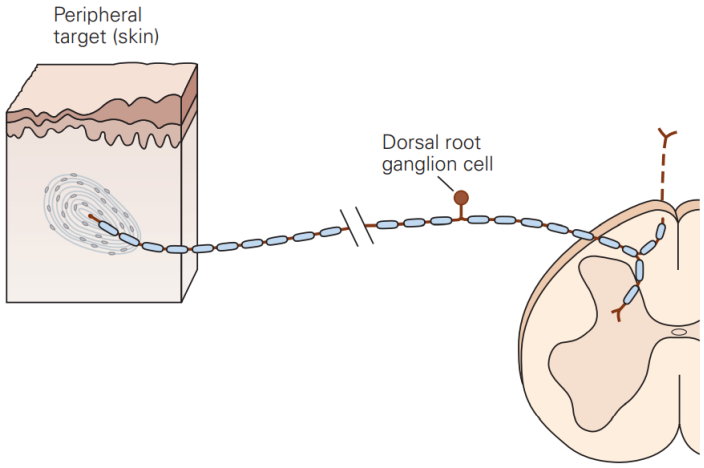

Figure 2.7 A segmental structure of the spinal cord and its pathway and root [1].

2.2.4 Dorsal Column Medial Lemniscal Pathway

The mechanoreceptive and proprioceptive information, for humans, is conveyed through the dorsal column lemniscal system [1]. In Figure 2.8, the pathway of the sensory information has been monitored. As it can be seen in Figure 2.8, every dorsal column has been separated into two main parts. The first one, by means of the medial septum, is medially edged, and the dorsal horn of the grey matter laterally bounds the second piece. The dorsal column is made up of cuneate (wedge-shaped) and gracile (slender) fascicles, and by their combination with gracile, cuneate, spinal trigeminal nucleus, and tract. When it comes to medial lemniscus, in the dorsal column, it is composed of axons of the neurons. By this, the midline is crossed in the medulla. In the medial lemniscus, due to the crossing, tactile information from the left side of the body is derived and processed by the right side of the brain [11]. Furthermore, the spinothalamic system conveys other information types such as chemoreceptive and nociceptive information [1].

The tactile information coming from the dorsal root is, firstly, reaches the spinal cord and then ascends the medulla. Later on, there has been a sensory decussation in the medulla, and the somatosensory information in the medial lemniscus ascends until arriving at the thalamus through respectively pons and midbrain. Eventually, it arrives

somatosensory cortex by tracts between the thalamus and somatosensory cortex [1].

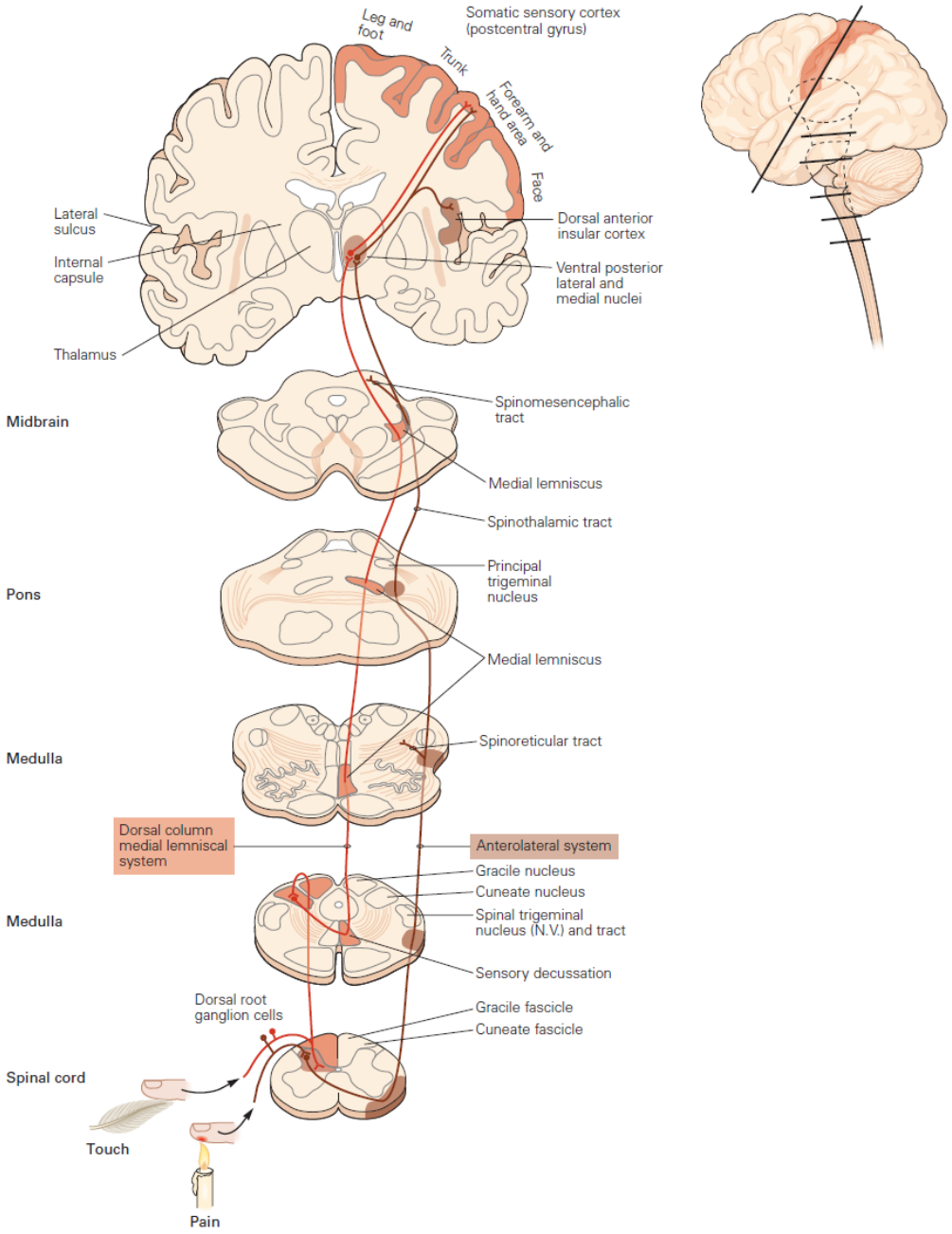

Figure 2.8 Pathway of the sensory information from trunk and limb [1].

2.2.5 Somatosensory Cortex

The somatosensory cortex is a cortex type that is mainly responsible for somatosensory processing at the most specialized levels and is located posterior to the

central sulcus of the parietal lobe in the cerebral cortex (Figure 2.9) [21]. The somatosensory cortex is, fundamentally, made up of three subdivisions that are posterior parietal cortex, the primary somatosensory cortex (S1), and the secondary somatosensory cortex (S2) [11].

Figure 2.9 shows that areas 5 and 7 lies on the posterior parietal cortex, the first of which is responsible for active touch. S1 extends from the central sulcus to the postcentral gyrus, and it contains Broadmann′s areas (1, 2, 3a, and 3b). Among those, while 2 and 3a collects and processes proprioceptive inputs, area 1 and 3b derive tactile inputs that are cutaneous [11].

The reason why area 3b corresponds to the proper somatosensory cortex has 4 causes. Firstly, somatosensory experiences are aroused when they are stimulated electrically. Secondly, if there has been a lesion, then it ruins the sensation of the somatic system. Another reason is that somatosensory inputs evoked its neurons since they are very responsive to such stimuli. Lastly, as mentioned before, it receives sensory information from the nucleus or nuclei of the ventral posterior VP system of the thalamus [11]. Moreover, the dense inputs transmit from area 3b to areas 2 and 1. Mainly, area 1 receives texture, and area 2 derives size and shape information of the object from area 3b (Figure 2.9) [1, 11].

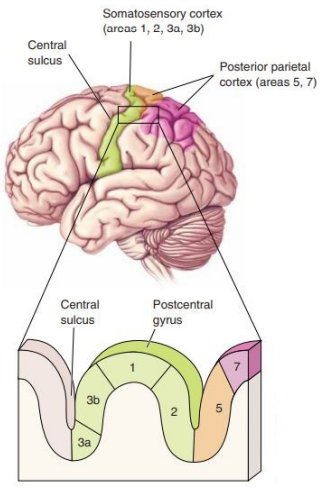

Figure 2.9 Somatosensory areas of the cerebral cortex [1].

In addition to Broadmann's areas, brain parts in the somatosensory cortex were separated into layers and columns by Vernon Mountcastle. According to his studies, every one of the columns has approximately 300-600 µm width and length. The same receptors are responded to by neuron groups in a column, and these neuron groups derive the neural information from the same receptor sheet area [1, 22].

Figure 2.10 displays simply somatosensory pathway from finger to area 3b of the somatosensory cortex and deep layers and columns of it. As it can be seen in the figure, from layer VI to layer I, there are some feedback and feed-forward connections to ascend the information. Layer I involves lateral transmission of the somatosensory information. Layer II and layer III conveys the neural activities to other parts of somatosensory cortex. The information in layer IV generally comes from the thalamus and is the main sensory input. Furthermore, layer V represents the neural activities that are transmitted to the spinal cord, brain stem, and basal ganglia, and eventually, layer VI transfers the information to the thalamus [1, 23, 24].

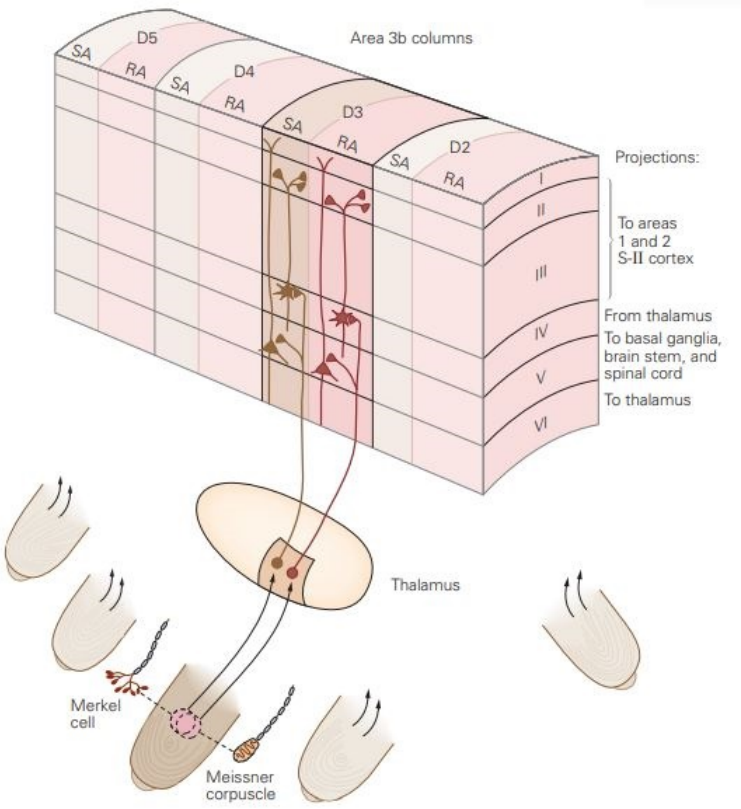

Figure 2.10 Columnar organization of the somatic sensory cortex [11].

The somatosensory information from receptors to the somatosensory cortex is transmitted through somatosensory pathways, which have feedback-feedforward connections and excitatory-inhibitory relay nuclei. According to Figure 2.11, these relays not only convey the sensory information but, from in presynaptic pathway, derive synaptic inputs that are excitatory and convergent, as well. Huge amounts of postsynaptic neurons are excited by single receptor neuron or neuron groups. Further, the ability to excitation of relay neurons is triggered by inhibitory interneurons in the relay neurons [1].

In Figure 2.11A, neurons in the relay nucleus in the receptors under the skin were monitored. In relay nuclei in the thalamus and brain stem, huge amounts of postsynaptic neurons modulate a stimulus to the skin [1]. Most of this process has occurred in central (red) neurons. Due to the convergent connections, any types of presynaptic neurons smaller than individual relay neuron′s receptive fields [25]. In Figure 2.11B, by improving adversity between stimulated relay neurons weakly and strongly, excitation (orange) is bounded by local interneurons mediated by inhibition (grey) to the central area [1]. Lastly, for Figure 2.11C, three different pathways of excitation evoke inhibitory interneurons in relay nuclei. Lastly, for Figure 2.10C, three different pathways of excitation evoke inhibitory interneurons in relay nuclei. Output neurons are inhibited by the interneurons, which produce inhibitory and excitatory activity in the nucleus. Additionally, in the output pathway from the nucleus, for neurons, collateral axons create feedback inhibition. Moreover, afferent receptive fibers create feedforward inhibitions. Sharply described zones by interneurons ensure the strategy of winner-take-all, which allows them to perform just one single response among more than one.

2.3 Psychophysical Theory

In neuroscience, one of the most ubiquitous topics is psychophysics. Psychophysics is a scientific research topic that is responsible for the relationship between perception and stimulus. The stimulus may be produced to evoke all sorts of senses

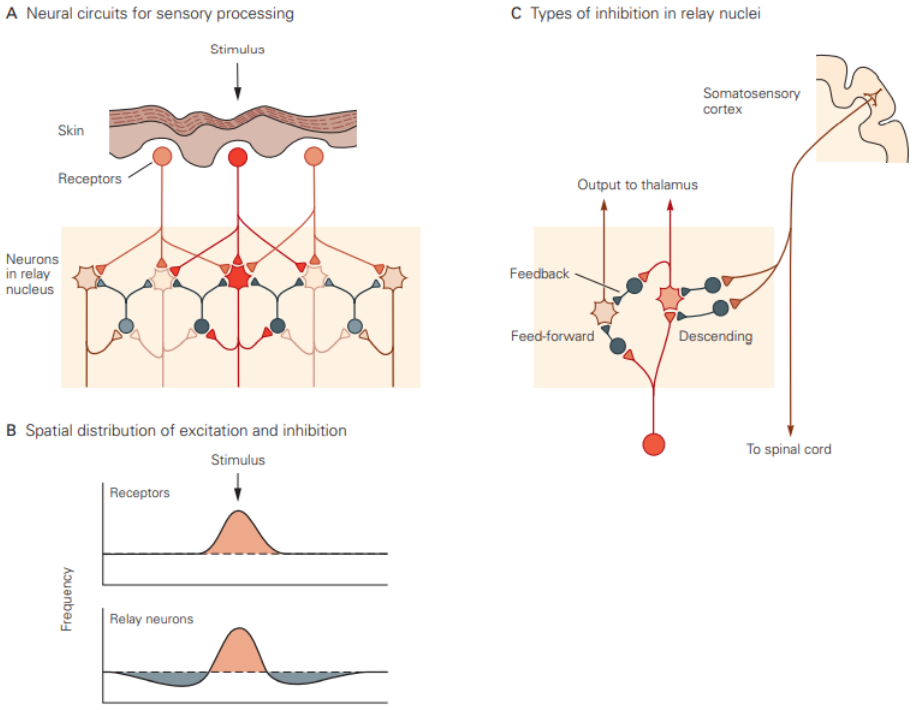

Figure 2.11 Completion of somatosensory activity from several receptors by neural connections in relay nuclei [1].

in the human body, such as smell, taste, touch, hearing, or vision. Discrimination, absolute threshold, and scaling are three fundamental concepts of psychophysics [26].

The absolute threshold is a boundary level that can be perceived by a participant depending on the absence or presence of the stimulus. Sensing difference or presence parameters are accepted as probabilistic, and therefore, the specific amount of proportion of correct responses produced by given stimulus level is assumed as the absolute threshold level in the field of neuroscience [26]. To derive a more accurate absolute threshold parameter, measures of the threshold should be averaged [26]. In the experiments, 75% correct probability of the trials is supposed to be an absolute tactile threshold. [27].

The absolute tactile threshold can be assumed as the minimum tactile perception level for an animal or human. Tactile perception, fundamentally, has 4 psychophysical channels mediated by receptive systems and which are called as Pacinian (P) channel and Non-Pacinian I (Meissner corpuscles), II (Ruffini endings), III (Merkel cells), or

NPI, NPII, and NPIII, channels [28, 19, 29, 30, 6, 17]. Among all those, the P channel has a minimum detection threshold level within the wide range between the frequency of 200 and 300 Hz [31, 17, 32].

In Figure 2.12, threshold levels of four mechanoreceptive fibers within the frequency range of 0.1-1000 Hz were shown. According to the figure, NPII is the least sensitive psychophysical channel for any frequency level. However, NPIII channel is the most sensitive channels below 2 Hz frequency and the NP I (Meissner corpuscles) is the most sensitive channel at 30 Hz vibrotactile stimulus. In this thesis, 40 Hz vibrotactile stimulation was used. According to previous literature, P channel may have lower threshold level than NPI channel at 40 Hz (Figure 2.12).

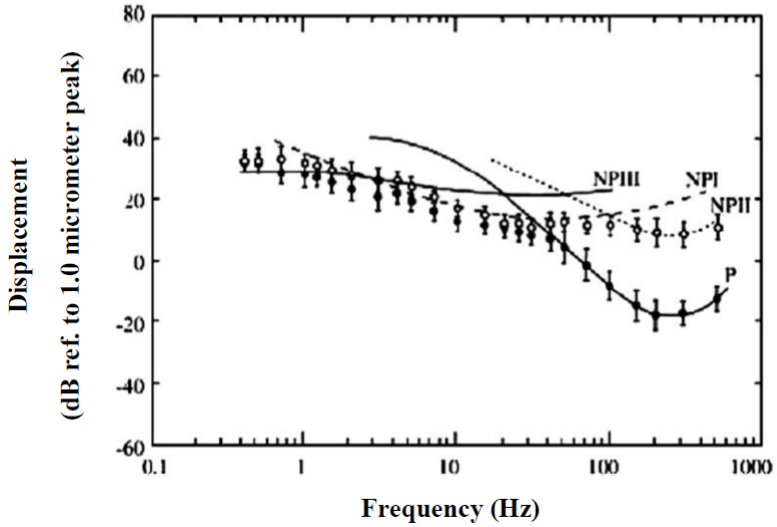

Figure 2.12 4 channels mechanoreceptive model between 0.1-1000 Hz [29].

2.4 Somatosensory Evoked Potentials (SEPs)

Somatosensory evoked potentials (SEPs or SSEPs) are spinal cord or brain responses, and they are namely recorded to evaluate the somatosensory pathway, which allows us to diagnose neurological disorders [33]. Typically, SEP recordings can be obtained by electrical stimulation to an ankle or a wrist of the individual body [34]. The potentials are collected from sensory areas of the cortex.

2.4.1 Somatosensory Potentials Evoked by Electrical Stimulus

Electrical stimulation for evoking somatosensory potentials is mainly rectangular pulses within a certain period. It has a good capability of activating numerous neurons. Precisely, in the literature, 5-15 electrical stimulation pulses (biphasic rectangular pulse duration of 0.2 ms) was applied to the median nerve. It was pointed out that the amplitude responses evoked by electrical stimulation (1 to 5 µV) were considerably higher than mechanical SEPs (0.25 to 1 µV). Electrical somatosensory evoked potentials are derived as three distinct parts, which are short-latency, mid-latency, and long-latency [35, 36]. Thanks to short-latency responses, we can study sub-cortical areas. By observing mid latency, the primary somatosensory cortex can be monitored. Additionally, the long latency may enable us to observe other connected cortical areas.

Figure 2.13 monitors the SEPs when the right arm of a human is exposed to stimulation. In the figure, there are 4 different potentials and are several types of peaks, either negative or positive, which are derived from different areas of the neck and head.

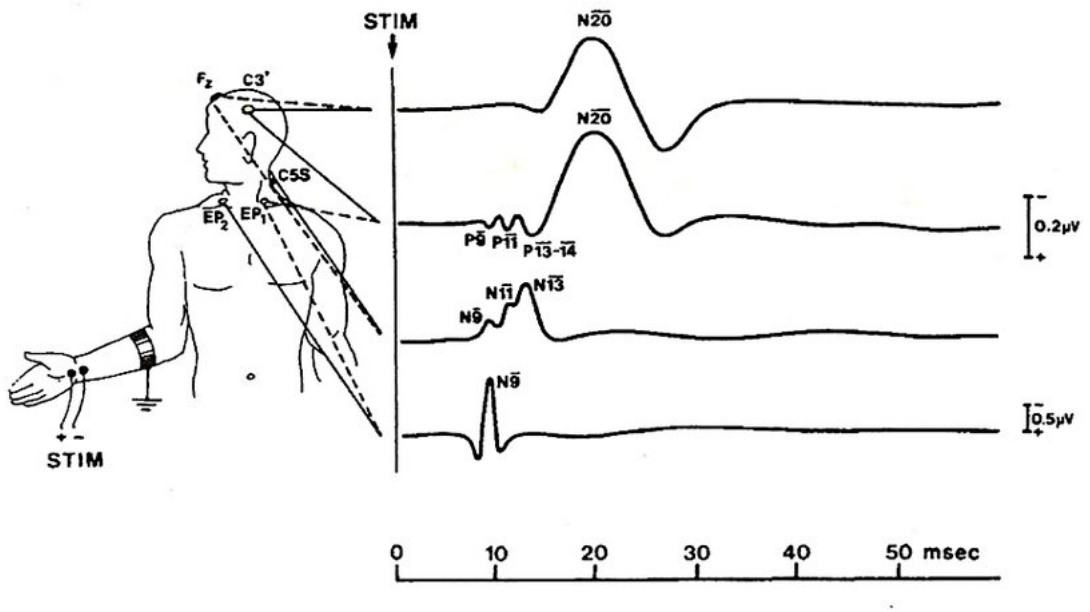

Figure 2.13 Electrical stimulation of the arm [37].

Furthermore, Figure 2.14 exhibits that there can fundamentally be five different peaks that are considered (N20, P25, N35, P45, and N50) and used to describe latency during observations [38].

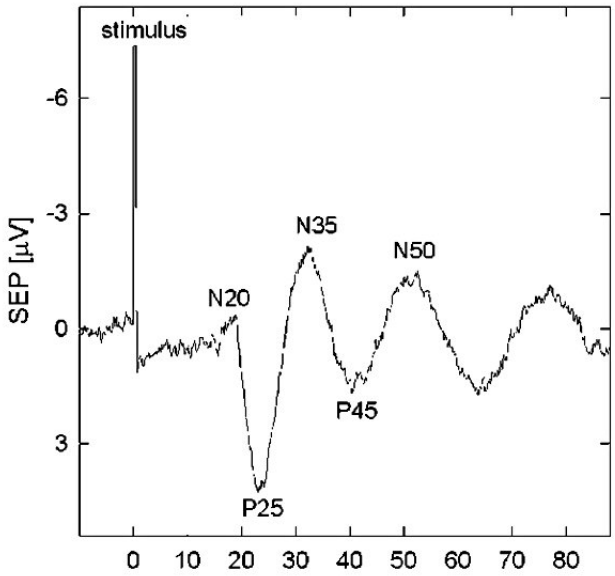

Figure 2.14 Somatosensory evoked potentials revealed by an arm stimulation [39].

2.4.2 Somatosensory Potentials Evoked by Mechanical Stimulus

As mentioned in the previous sections, Although SEPs evoked by the electrical stimulus is robust in terms of responsivity, they may enable a restricted amount of knowledge such as relative contributions and velocity of transmissions of groups of fibers [40]. On the other hand, mechanical evoked SEPs are good at monitoring the information processing for tactile sensory feedback, thanks to their intrinsic characteristics. Specifically, realistic or natural stimulations should be used, so electrical stimulation is not required for human nature. Hence, conducting tactile stimulus-based studies is extremely important in order to understand natural SEP responses. Even more, there are a lot of studies about electrically evoked somatosensory potentials on human subjects and their apparent peaks or components. However, there is very little research on SEPs evoked by mechanical stimulus and the still gap in the literature. The reason for this may be related to being a low pass (LP) filter feature of the human scalp so that the certain frequencies or amplitudes knowledge could be suppressed.

As an example for mechanical SEPs studies in literature, brain responses were derived from the cortex by using many non-invasive electrodes for 33 Hz vibrotactile stimulation. When they observed temporal responses, they could not observe certain peaks in time and strong correlations could not be found. However, some prominent peaks could be observed by looking frequency domain information (Figure 2.15) [41, 42]. In Figure 2.15, the somatosensory responses of different areas of the brain triggered by mechanical stimulation were shown. According to the figure, anterior represents frontal, but posterior represents back areas of the brain. Medial is middle, and the lateral is side-ward. Additionally, the C3 area is our main recording area for somatosensory recordings. One of the fundamental aims of this thesis study is to observe the somatosensory response by using a non-invasive recording method and analyzing the data in both the time and frequency domain simultaneously. This is because, there are currently no strong results to show clear time-domain peaks for mechanical SEPs in literature.

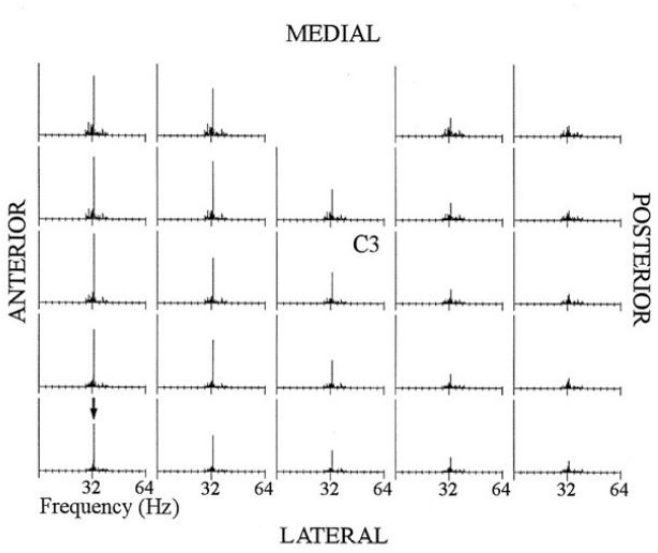

Figure 2.15 Somatosensory potentials evoked by mechanical stimulation [41, 42].

2.5 Time Domain Analysis

Briefly, time domain analysis is a signal analysis method that focuses on the amplitude information of a signal with respect to time. Recently, in order to interpret the brain data, non-linear techniques and EEG methods have been ubiquitously used [43, 44]. Among them, the former was not considered in this thesis since non-linear analysis methods are generally used to observe a restricted amount of neuronal (for single or just a few neurons) activity. On the other hand, EEG methods are one of the well-known methods to analyze brain data within a certain brain area.

Electroencephalography (EEG) is a dynamic response of the CNS. In order to gather clear results, its recording is needed to be paid careful attention. The method may enable us to analyze the data in either time (as a voltage) or frequency (as an amplitude) domains. EEG signals are observed as EEG bands by filtering the original (raw) data, and each band carries divergent information. In other words, various wide or narrow bands of EEG responses are generated by the human brain when the brain of an individual in the different brain states (e.g., concentration, active mind, or sleep) [45]. When an individual undergoes a vibrotactile stimulus, a higher frequency of 90 Hz and lower than 4 Hz brain responses are not considered much for EEG signals resulting from mechanically vibrational stimuli and, generally, the former of which is filtered by low pass (LP) filters and the latter one is eliminated by high pass (HP) filters by means of signal processing methods.

Although there are much more narrow EEG bands, just a few of them are assumed as fundamental EEG bands, which are delta (0-4 Hz), theta (4-7 Hz), alpha (8-12 Hz), beta (12-30 Hz) and gamma (30 Hz and up) [45, 46]. Among those bands, the delta band is associated with dreaming and sleep. The theta band can be associated with deeply relaxing or snoozing. The alpha band exhibits passive attention and restfulness. The beta band may represent the external attention and active mind, and lastly, the gamma band can be correlated with concentration and problem-solving (Figure 2.16) [46]. In this thesis, delta and theta bands were not included due to being associated with sleep or dreaming and snoozing or relaxing.

Although EEG is one of the proper ways to observe the brain data, its bands in the time domain could not show us clear information or apparent peaks, as seen in the figure (Figure 2.16). Figure 2.16 shows raw EEG data and its fundamental bands in the time domain for 40 Hz vibrotactile stimulation for one human subject by using mechanical stimulation and non-invasive recording for 1000 ms time duration [8]. Stimulus starts at 0.2s and last for 0.5s. According to this figure, it appears there are no changes related with the stimulus in the time domain for specific intervals of time. They seem to be randomly distributed. Even if raw EEG data were separated into narrow bands, there are no exact prominent peaks that were able to be observed for SEPs upon mechanical stimulation by only looking at its time-domain information.

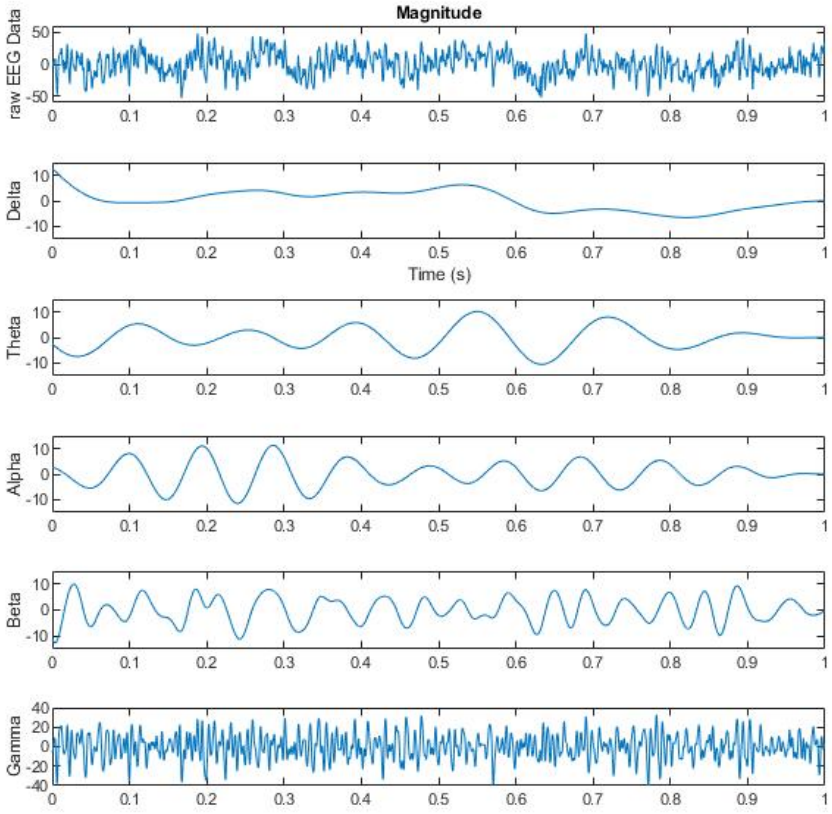

Figure 2.16 Raw EEG data and its delta, theta, alpha, beta, and gamma bands in time domain.

2.6 Frequency Domain Analysis

The SEPs can be transformed from time into frequency domain responses in order to collect the information or verify the hypothesis in neuroscience, particularly in computational neuroscience. Frequency domain analysis is, mainly, to transform the amplitudes of a signal from the time into the frequency axis. By doing this, the amplitude spectrum of a signal may be observed for various frequencies. In other words, they are the sinusoidal representation of a measured or original signal. In math, the common way is the Fourier transform method to represent measured data by sinusoids.

In several studies, it has been displayed that adequate duration of periodic vibrations was able to result in spike activities in the primary somatosensory area (S1 cortex), which could be observed by MEG or EEG recordings [47, 48, 49]. Specifically, 20 Hz repetitive mechanical stimulations on human fingertips for 1s duration with 5 seconds time interval and magnetoencephalogram (MEG) for recordings of the brain responses were used. They have concluded that vibrotactile stimulations lead to oscillations of the S1 cortex [47]. In another study, 75 Hz mechanical vibrations on human upper limb and EEG recordings were considered, and the results showed that the S1 cortex could be excited by mechanical stimulations. Even more, it was also proved that mechanical vibrations on the skin could evoke brain responses on the S1 cortex by means of EEG recordings [49].

Even though there are numerous studies, recently, in terms of the effect of mechanical stimulus or vibrations on the S1 cortex, yet still, the impact of 40 Hz vibrotactile stimulation at psychophysical threshold and suprathreshold levels (up to 30dB SL) could not be found by only considering the frequency domain analysis (e.g., cross-correlation, FFT, etc.) methods. In Figure 2.17, the frequency domain information of an EEG signal was shown. The signal represents EEG response taken by the non-invasive recording of a subject for 40 Hz mechanical stimulation of human skin [8]. The figure shows that narrow bands (delta, theta, alpha, and beta) are not able to carry a sufficient amount of information, and any prominent peak cannot be observed for any band similar to the time-domain analysis. It means that collecting only fre-

quency domain information of the signal and its bands may not be sufficient to analyze brain data. As a result, likewise time, only frequency domain information is not a solution to show the clear information. Hence, using both time and frequency knowledge simultaneously may be required to analyze mechanically evoked human brain data.

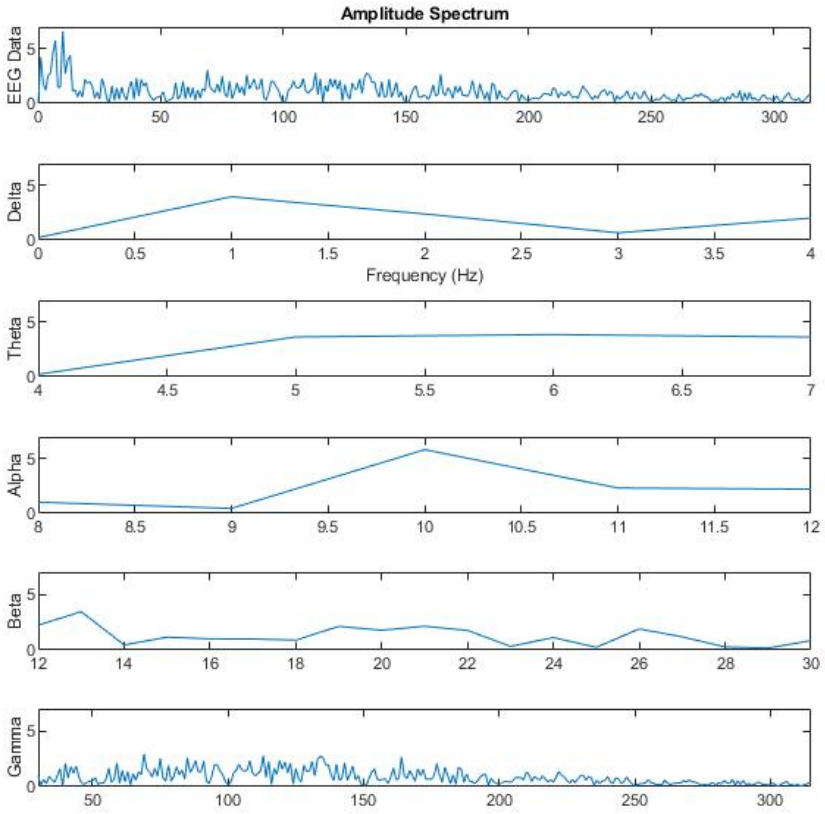

Figure 2.17 EEG data and its delta, theta, alpha, beta, and gamma bands in frequency domain.

2.7 Time-Frequency Information Derived by Signal Processing Methods

Signal processing is a mathematical way used to analyze electrical signals in various fields such as neuroscience as well as engineering. In neuroscience, signal processing and its algorithms are considered as it is one of the quintessential and widely

used methods in order to transform complex physiological signals into noteworthy pieces of information [50]. Specifically, this method is used in terms of analyzing auditory (AEPs), visual (VEPs), and somatosensory evoked potentials (SEPs), and whole those signals are assumed as responses of the brain undergo several stimulus types (e.g., electrical stimulus transmitted to a nerve, visual pattern change, flash of light, click, and the burst of tone) [44]. Furthermore, evoked potentials (EPs) should be extracted a lot of times and averaged since when they are collected trial-by-trial, their magnitude responses are really lower compared to background noises, and averaging step boosts the amplitudes sufficiently [44]. In literature, many studies were monitored that signal processing methods as a thorough way to extract expected knowledge in neuroscience for all EP types.

In practice, There are several signal processing techniques depending on the dimension (e.g., 1D, 2D, and 3D) of the data used to derive neural data. For instance, wavelet transform and filter-Hilbert can be considered to analyze 1D and 2D signals. Fourier transform (FT) and filter-Hilbert are able to be used for 2D signals. Even more, tensor decomposition and multidimensional signal processing methods are good methods for reconstruction and analysis of 3D or more dimensional signals respectively. In this thesis, because of our data is 2D, FT, filter-Hilbert, or Wavelet Transform (WT) can be considered. Among those filters, in this thesis, WT method was chosen instead of FT or filter-Hilbert.

This is because FT may give amplitude information of the data with respect to the only frequency information. However, observing time and frequency information of a signal at the same time may sometimes be more important for brain signals. WT has the ability to exhibit all these features of such data simultaneously [51, 52, 53]. FT leads to global uncertainty in the signal, which cause of being less informative for the non-homogeneous signals such as brain signals; however, WT may cause regional uncertainty in small regions, and this allows the signal to give knowledge in terms of every one of the fragments of the signal [51, 52, 53, 54]. Even more, EEG signals are accepted as non-stationary, which means statistical properties of these signals may alter in the time in the literature, and FT is usually an appropriate method for stationary

signals, but it is insufficient for analyzing non-stationary ones. Conversely, WT is pretty capable of observing those signal types [51, 52, 53, 55].

Apart from FT, filter-Hilbert method was not considered since although this method may produce accurate frequency domain results, it generates highly energetic signals at each time or frequency point, which makes the results uninterpretable. In other words, it has only empirical results only if the data are narrowband signal [56]. Hence, this method is required to be used after implementation of a bandpass (BP) filter. Compared to WT, filter-Hilbert takes more time since it includes several Fast Fourier Transforms (FFT) inside, and it is required a preprocessing step (bandpass filtering), as mentioned. On the other hand, WT is needed just a few FFT, so its implementation is absolutely easy and rapid [57].

2.8 Time-Frequency Analysis (TFA)

By using WT, data can be segmented or windowed into tiny fragments on the entire spectrum (Time-Frequency Plane). The length or width of every single window, or called as Heisenberg box, defines the resolution of frequency or time of the information. Just like Heisenberg′s uncertainty principle, if the time resolution of the signal is increased, the resolution of the frequency information needs to be reduced proportionally (Heisenberg Box 2). On the other hand, if one would like to collect high-resolution frequency information, then the time information should be lowered in terms of resolution (Heisenberg Box 1) (Figure 2.18) [58].

Simply put, Time-Frequency analysis (TFA) is a signal analysis method that may enable us to observe amplitudes corresponding to time and frequency plane at the same time unlike time or frequency domain analysis methods. Its thorough feature is ability to monitor the whole concept at only one plot. There are various time-frequency plots that are used for signal analysis such as multiresolution analysis (MRA), Constant-Q Gabor transforms, reassignment and synchrosqueezing, Wigner-Wille distribution (WVD), spectrogram (short-time fourier transform), and scalogram (CWT:

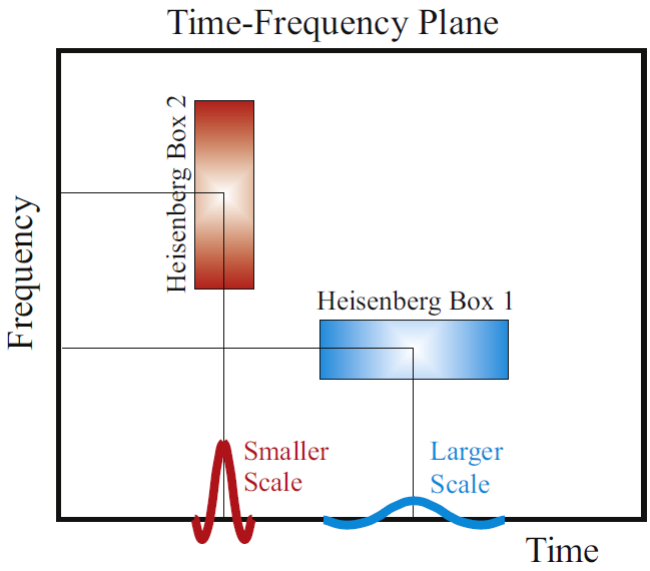

Figure 2.18 Heisenberg uncertainty boxes on the Time-Frequency Plane [44].

continuous wavelet transform) [59].

Among those, MRA is mostly used for discrete analysis, and constant-Q Gabor transform is a good way for processing music signals. For the reassignment and synchrosqueezing method, it has been shown that oscillations of seismic or earthquake vibrations and power systems could be analyzed by this method [60, 59, 61]. The WVD technique is good at processing the sounds of cochlear origin undergoing auditory stimulations, and spectrogram can be considered to analyze audio signal processing such as Pacific blue whale [59]. On the other hand, for either processing physiological (particularly ECG or EEG) signals or considering CWT, scalogram-based time-frequency analysis is taken into account [62, 59]. Hence, in this thesis, a magnitude scalogram plot was chosen in order to monitor whole amplitudes with respect to the time-frequency information.

2.8.1 Wavelet Transform

Wavelet transform is, simply put, a signal analysis method that mainly enables us to use in data compression, feature extraction, and signal processing [63, 64, 65]. Its

usage areas are formed only for a couple of decades although it has been accepted mathematically approximately for a hundred years [44]. Its ability to show non-stationary brain responses makes this method unique when it comes to observing physiological (e.g., MRI, PET, ECG, or EEG) data compared to conventional signal processing techniques [66]. By means of wavelet analysis, frequency-domain knowledge of the signals can be obtained like FT or filter-Hilbert. It may give information about where a specific frequency reveals in the spatial or temporal plane.

Wavelet analysis can be performed in both discrete and continuous time domains. According to Table 2.1, all WT types provide the time-frequency plane with a center frequency which is a logarithmic one. Moreover, discrete type wavelets, which are wavelet decomposition (WAVEDEC), DWT, maximal overlap DWT (MODWT), have only one wavelet-filter/octave and 2 bases, but CWT differs from others in terms of generally having 8 or 16 wavelet filters per octave and $2^{1/NV}$ (NV is number-of-filter/octave) bases. Moreover, the time shift of the WAVEDEC, DWT, and CWT is 1 sample, but for MODWT, there are 2^L (L represents a level of DWT). In addition to those features mentioned in Table 2.1, Continuous wavelet transform is ubiquitous for harmonic signal analysis thanks to its ability to conserve the phase information of the signal [67, 44]. In other words, highly fidelity analysis can be obtained for signals by means of its thorough feature, perfect monitoring the characterization of the oscillatory mechanisms, compared to discrete ones when the proper sampling frequency is considered, which makes the CWT is a perfect and appropriate method to analyze such signals in this thesis [68].

Table 2.1
Fundamental differences and similarities among main WT types [69, 70]

Method	Wavelet Filters per Octave	Logarithmically Space Center Frequency	Base	Time Shift
WAVEDEC, DWT	1	Yes	2	1 Sample
MODWT	1	Yes	2	$2^{(L)}$ Samples
CWT	Mostly 8-16 practically	Yes	$2^{(1/NV)}$	1 Sample

2.8.2 Continuous Wavelet Transform (Scalogram)

Scalogram or magnitude scalogram is a time-frequency plot that displays amplitude and time-scale by the implementation of the CWT in MATLAB [71]. It has many application fields, two of which (ECG and EEG) are very well-known. CWT is considered as such a proper method in terms of monitoring the signals if their instantaneous frequency fastly ascends or intuiting transients in the non-stationary signals [59]. In neuroscience, there are three most common problems such as raw EEG signals have numerous artifacts, a very small amount of signal-to-noise (SNR) ratio, and insufficient spatial resolution for neuroscientists encountered [59]. By using thresholds for wavelet coefficients, the SNR ratio can be enhanced since even if there are only a few large valued CWT coefficients, consistent peaks could be extracted with no random distribution adjusting of noises [59].

Scalogram plot can be constructed by using three analytic continuous wavelet types provided in MATLAB, bump, analytical Morlet [72], and generalized Morse [73, 74] (Figure 2.19). Among these wavelets, bump wavelets are more strict in time, but they are broader in the frequency domain compared to others in terms of variance [75]. On the other hand, the frequency variance of the Morlet wavelets is the same as their time variance. In other words, their time and frequency variances are fixed. On the contrary, generalized Morse wavelet has changeable two (compactness and time-bandwidth) parameters in order to change frequency and time dissemination [75]. This unique characteristic enables Morse wavelet to exhibit Morlet or Bump like behavior by just changing these parameters [76]. Even more, for the brain signals, each time and frequency fragments can sometimes be important to make deductions from the data. Hence, it has the ability to evaluate and monitor a well spectral estimation of the brain responses at every one of the time-frequency planes between 1-2048 Hz in the frequency axis and from before stimulus to after stimulus in the time axis [75, 73, 77]. Therefore, in this thesis, the Morse wavelet method was preferred to transform the EEG signals. Furthermore, in literature, there are several studies shown before about processing EEG signals and plotting time-frequency plots by using Morlet wavelets [78, 79, 80, 81, 82, 83], but very few amounts of research carried out by means of Morse

[84, 85].

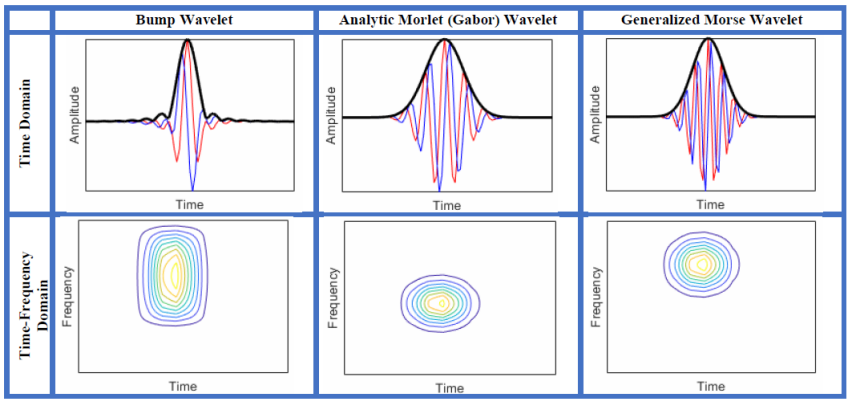

Figure 2.19 Time domain and Time-Frequency domain plots of the Bump, Analytic Morlet (Gabor), and Generalized Morse Wavelet respectively [75].

Morse Wavelet is a wavelet analysis method which has complex values. Only if a signal is in the real axis, Fourier transform can be performed for these complex values. Morse Wavelet was theorized, firstly, by Olhede and Walden [73], and its application fields were enhanced by Lilly, and Olhede [86, 87, 88]. Moreover, Lilly established an effective computer algorithm of the Morse wavelet and defined features of them [89].

For Morse wavelet, fourier transform demonstration is,

$$\Psi_{P,\gamma}(\omega) = U(\omega)\alpha_{P,\gamma}\omega^{\frac{P^2}{\gamma}}e^{-\omega^{\gamma}} \tag{2.1}$$

where $U(\omega)$ characterizes unit step function, $\alpha_{P,\gamma}$ symbolizes a constant of normalization, P^2 indicates time-bandwidth product, and γ represents Morse Wavelet′s symmetry feature. In most of the literature, instead of the time-bandwidth product, compactness parameter β is considered, so the equation need to be organized as [86],

$$\Psi_{\beta,\gamma}(\omega) = U(\omega)\alpha_{\beta,\gamma}\omega^{\beta}e^{-\omega^{\gamma}} \tag{2.2}$$

In the equation, symmetry parameters and product of time-bandwidth for Morse wavelet may allow us to derive various featured analytic wavelets. In order to do this, these parameters should be altered in requested values. Figure 2.20 and Figure 2.21 exhibits time and time-frequency domain knowledge derived by changes in P^2 and γ parameters, respectively. Specifically, it is assumed that the duration of wavelet in time is proportional to the P value [90]. At a certain frequency region, or called peak frequency, the number of oscillations that fit into center window of the wavelet in the time-domain has regulated by the duration. Formulation of the peak frequency can be shown as $(\frac{P^2}{\gamma})^{\frac{1}{\gamma}}$ [90]. According to this equation, if the γ parameter is adjusted as 3, the least number of Heisenberg Boxes will be composed, and the Morse wavelet's skewness will be equal to 0; therefore, this value can be assumed as default in MATLAB [90].

As it can be seen in Figure 2.20, long-time decay is increased when the P^2 is ascended if the γ becomes equivalent or lower amount than 3. For the γ parameters bigger than 3, when the P^2 is diminished, the wavelet information has become more asymmetrical [90].

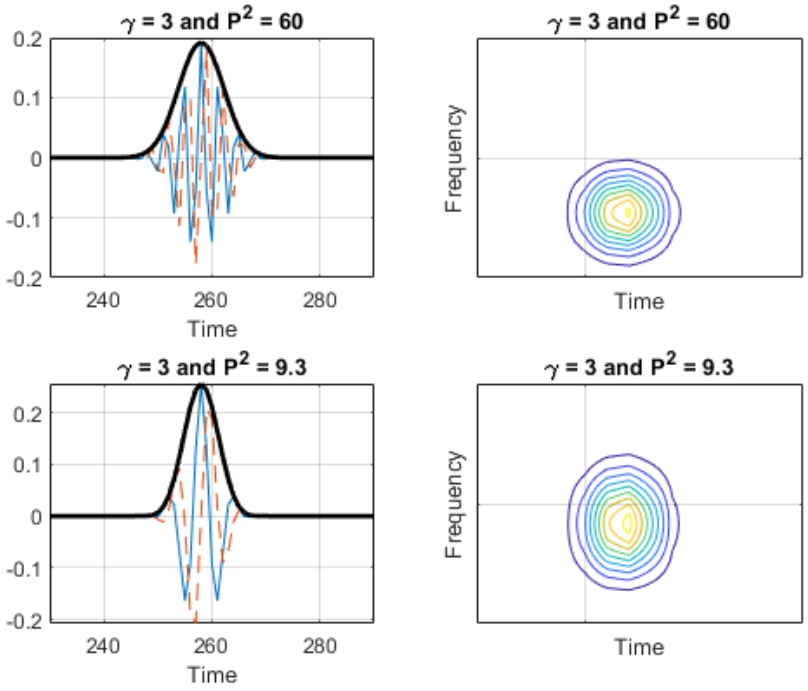

Figure 2.20 Changes in time and time-frequency knowledge of the signal when γ are same, but P^2 is altered [90].

Figure 2.21 signalizes that long-time decay rates can be ascended when the P^2 is reduced. However, the increases in the γ parameter do not cause any change in time decay. That is to say, unexpected time lobes in the time domain and asymmetry in the frequency domain are generated by means of the higher level of γ and lower amounts of P^2. Furthermore, in frequency and time axis, the wavelet may lead to more oscillations when P^2 and γ becomes larger [90].

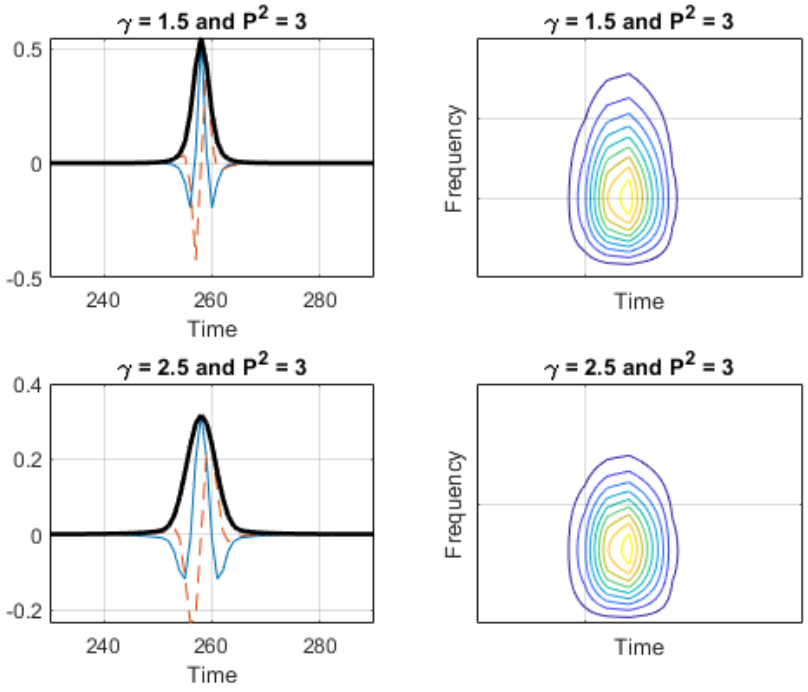

Figure 2.21 Changes in time and time-frequency knowledge of the signal when P^2 parameters are same, but γ is altered [90].

2.9 Research Question

The background knowledge mentioned in the previous sections was elaborately demonstrated. The purpose of this is to show the impact of SEPs on the somatosensory cortex by applying 40 Hz mechanical vibrations on the human fingertip. At threshold level, probably P channel is activated primarily. However, at suprathreshold levels, P, NPI and NPIII channels could be activated. One of the substantial aims of this study is to observe this effect by using mechanically evoked SEPs. This is because they enable us to produce mechanical stimuli which are close to a natural stimulus, which boosts

the possibility of collecting more empirical results. Moreover, data were analyzed using CWT by Morse wavelet since it has certain advantages over other FT or filter-Hilbert methods. Eventually, one of the fundamental goals of this research is to determine if the stimulus intensity and time window (TW) have a significant effect on studying somatosensory processing. This is because it may contribute to the literature of tactile sensory feedback in BMIs studies to be designed advanced neuroprosthesis. In order to verify those, the following experiments were carried out by Yildiz (2013) and analyzed by FFT, cross-correlation, and time-domain analysis methods [8]. However, significant correlations could not be found in previous studies. Therefore, the same EEG data were analyzed in more detail by TFA in this thesis.

3. METHODS AND PROCEDURES

The experimental data used in this thesis were collected by Yildiz (2013). In the experiments, mechanically evoked SEP responses were taken from seven subjects using 40Hz and 230Hz vibrotactile stimulations in four different sensation levels (NS, SL10, SL20, and SL30 dB). Both 40Hz and 230Hz data were analyzed by FFT, and Complex Morlet Transform [8]. Since significant results could not be found for 40Hz data, subsequent analyses were performed in this thesis.

3.1 Participants

Seven healthy adults (three male and four female), between 22-29 age, participated in the experiments [8]. The reason for choosing young participants is that aging has a negative influence on the sensitivity of vibrotaction [91]. To test individual participants, the experiments adhered to NIH ethical guidelines, and they were approved by the Ethics Committee for Human Subjects of Bogazici University. By self-report, it was informed that all participants were right-handed, so their middle fingertips of left hands were mechanically stimulated. The mechanical was very weak and did not cause any harm.

3.2 Experimental Setup

3.2.1 Apparatus

All experimental procedures were carried out in a vibration and soundproof room (RE-242, ETS-Lindgren Acoustic Systems, Cedar Park, TX). Firstly, by a computer and its connection with a digital-analog-converter card (DaqBoard/2000, IO Tech, Cleveland, OH), waves of the stimuli were produced. By using a PA5 digital attenuator

(Tucker-Davis Technologies, Alachua, FL), the intensity of the stimuli was regulated. In order to drive the mechanical shaker, adjusted signals were amplified by means of an RA300 power amplifier (Alesis, Fort Lauderdale, FL). Then, by driving of V203 electro-dynamic shaker that has a cylindrical probe (radius = 2mm) without surround (Ling Dynamic Systems Ltd., Royston, Herts, UK), the left middle fingertip of human participants was mechanically stimulated (Figure 3.1).

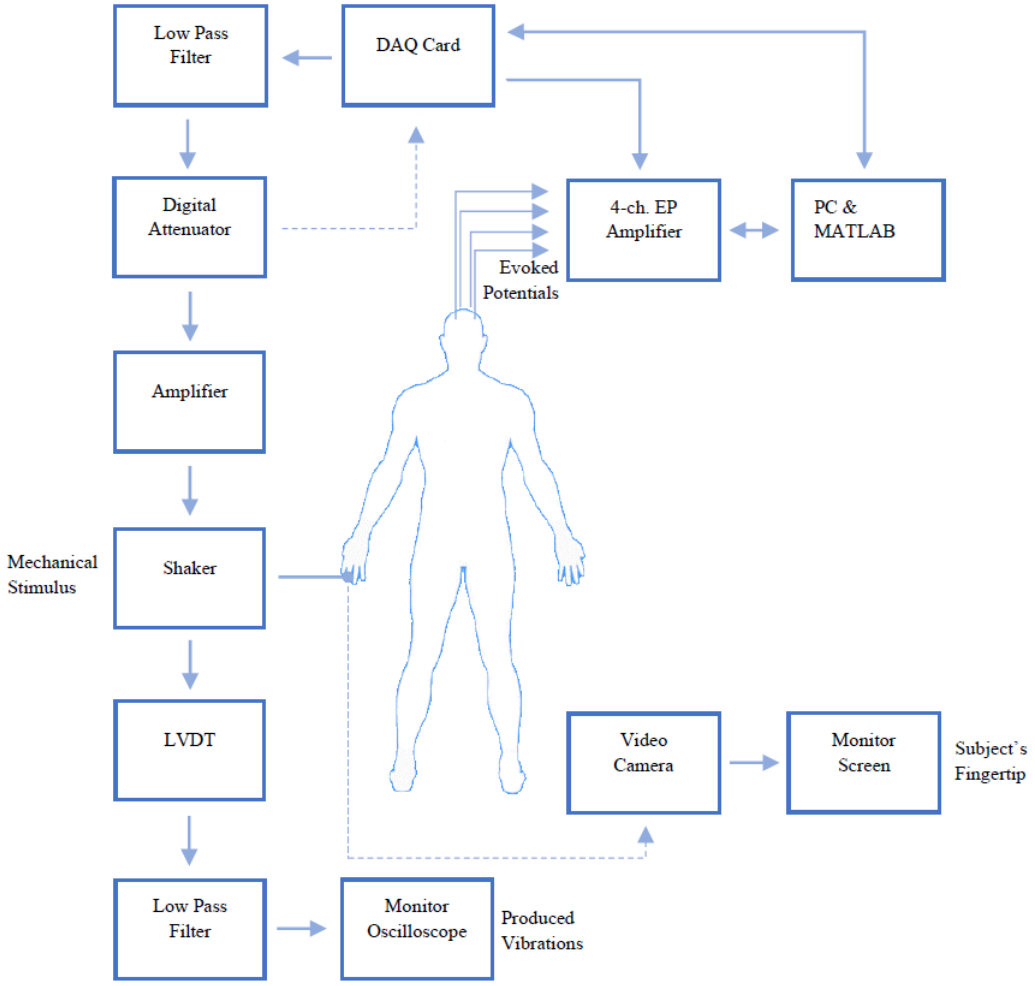

Figure 3.1 The block diagram of the experimental setup

In Figure 3.1, by using a Schaevits ATA2001 LVDT (Lucas Control Systems, Pennsauken, NJ) and TDS 2014 digital oscilloscope (Tektronix, Inc., Beaverton, OR), produced vibrations were measured and displayed, respectively. By modeling clay, the finger of the participants was stabilized to avoid shaking of the fingertip, which was observed during experimental protocol by a CCD video camera and projected onto a monitor. During the procedure, continuous auditory white noise was applied to the

subject by using a headphone in order to mask the noises of the shaker. By using a response box that was custom made, subject responses were collected, and finally, by means of a portable evoked potential amplifier (Micromed System Plus), evoked potentials were recorded.

3.2.2 Stimuli

As it can be seen in Figure 3.2, the stimuli are made up of vibrations that have cosine-squared ramps of 50 ms rise/fall times. The duration of each was 1 second and evoked potential recording was performed throughout the trial. The stimulus duration was 0.5s. The stimuli are formed by enveloping the burst sine waves of distinct magnitudes. The stimulus started 0.2s after the beginning of the trial. The timing diagram in Figure 3.2 applies to the evoked potential measurement step described below.

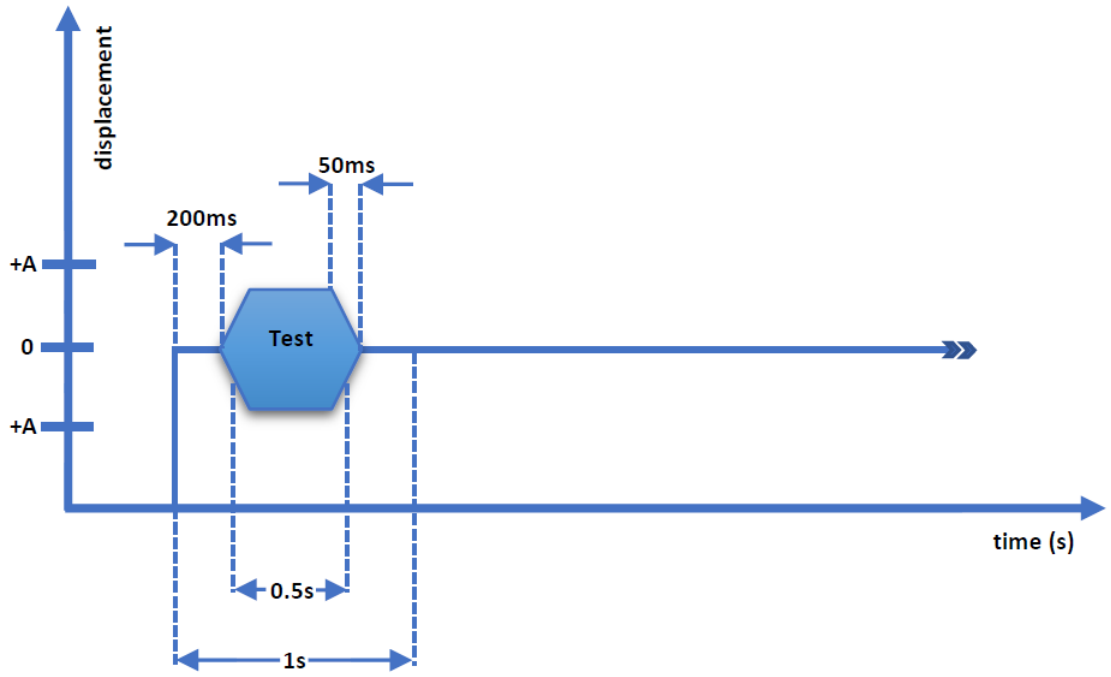

Figure 3.2 Stimulus timing diagram of the experimental procedure

3.3 Experimental Protocol

The experimental protocol was constituted of two fundamental steps, the former of which is psychophysical threshold measurements, and the latter is the SEP recording step. In the first step, an unmasked stimulus was applied to the participants at 40 Hz frequency in a psychophysical detection task. After the first step, SEP recordings were obtained at various stimulus intensity (NS, SL10, SL20, and SL30 dB) levels at 40 Hz.

3.3.1 Psychophysical Procedure

During experiments, a psychophysical procedure was performed initially. This procedure consisted of a two-interval forced-choice task, which included adaptive tracking (three-down one-up for not necessarily consecutive correct responses) rule. By doing this method, their tactile thresholds were evaluated without any criterion of participants. For this procedure, after every three correct answers, the stimulus amplitude decreased 1 step; on the other hand, after every wrong choice, the intensity was increased 1 step. This up-down rule was repeated until the average of the last 20 trials within ± 1 dB range for all subjects. At the end of this psychophysical procedure, within this range, were recorded. During the procedure, the subject selected the interval in which he or she sensed the stimulus. The stimuli were randomly presented either in the first or second interval at every trial for threshold measurements at 40 Hz stimulus.

3.3.2 Recording of Evoked Potential

During this step of the whole experiment, four electrodes were placed on the scalp over the head, two electrodes placed over the forehead, and the other two placed over the somatosensory cortex. Mechanical stimuli for the evoked potential procedure were similar to those used in the threshold measurements. However, their amplitudes were increased referenced to the threshold (sensation level: SL). All EPs were averaged

100 times, and the recording duration was about 1s. For recordings, the sampling frequency was adjusted to 2 kHz. In Figure 3.3, for the stimulus, CH1 was considered as the test channel and CH2 for the control. CH1 data were collected by the difference of the potential coming from two electrodes placed over contralateral (Cpc) and ipsilateral (Cpi) on the human scalp. Cpi was attached to the negative end, and Cpc was attached to the positive end of the amplifier. For four amplitude levels (no stimulus (NS), SL10, SL20, and SL30 dB), the experimental protocol was repeated.

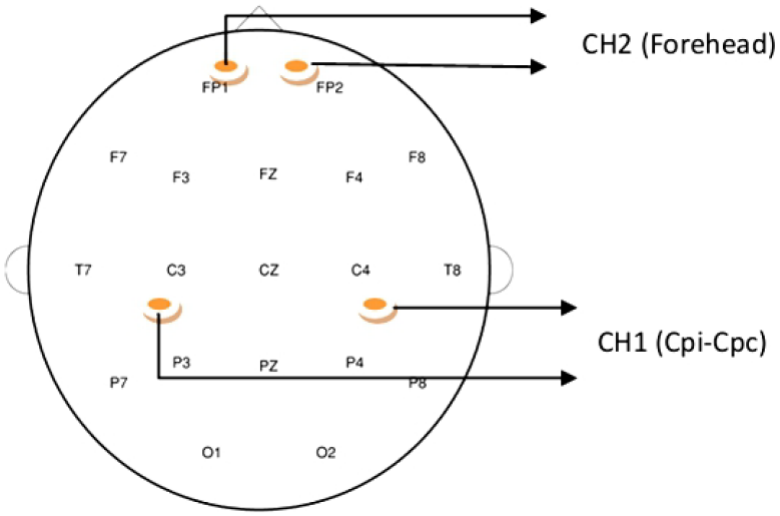

Figure 3.3 Measurement diagram of the SEP [8].

3.4 Analyses

During analysis, firstly, raw EEG data or SEP responses of all subjects for CH1 and CH2 were monitored corresponding to the time. Secondly, the signals were projected onto the frequency domain. In the frequency domain, firstly, the CH1 data of each (7 subjects) subject was subtracted from its CH2 data and obtained for 4 different SLs. Afterwards, CWT was performed with Morse Wavelet Transform by taking $\gamma = 3$ and $P^2 = 60$ and almost 10 bandpass filter per octaves in MATLAB [92]. The average Time-Frequency plot was produced and displayed as a magnitude scalogram plot with respect to the time and frequency axes by taking the subject average from those 4 SLs.

In addition to the scalogram plot, wavelet coefficients were averaged in the time and plotted as EEG bands with respect to the frequency to find overall EEG band knowledge as wide-band (8-314 Hz). After that, the wide-band was separated into small fragments as other EEG bands, alpha-beta (8-32 Hz), stimulus band (32-48 Hz), low gamma (32-90 Hz), high gamma (90-314 Hz), and TWs (*Ro* comprises 0.2-0.3s or the first 0.1s of the stimulus period recording period and Rd^* contains 0.3-0.7s or last 0.4s of the stimulus duration). Lastly, the overall energy corresponding to time and frequency was evaluated and statistically analyzed.

Statistical analyses were performed using the SPSS Statistics 27 computer program. For the average amplitudes of the Rd^* and *Ro* scalogram difference data, two-way repeated-measures ANOVA was applied to the data with the within-subject factors of sensation level and frequency band. To test within-subject effects, sphericity assumed parameters were considered, and significant parameters were listed. Finally, in order to collect post-hoc results, tests of pairwise comparisons were carried out by Fisher′s Least Significant Differences in estimated marginal mean, and significant results were noted.

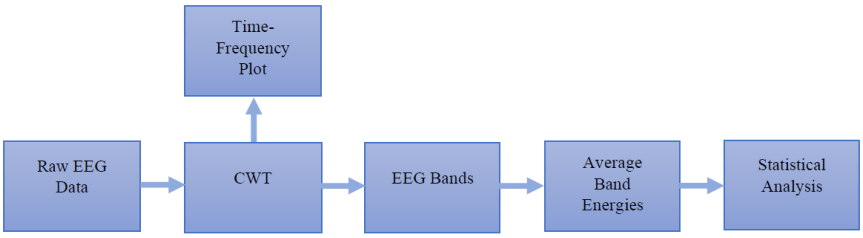

Figure 3.4 Block diagram of the signal analysis steps

4. RESULTS

4.1 Mechanical SEP Responses

In this section, raw data (mechanical SEP responses) outputs of all subjects for two channels were shown (Figure 4.1 and Figure 4.2). The following signal processing and statistical analysis were conducted by using these data. Figure 4.1 monitors SEPs responses of the CH1 (test) channel, and Figure 4.2 represents SEPs of the CH2 (control) channel. Only for the S1 subject, SL10 data were excluded after experiments for both channels.

As it can be seen in Figure 4.1, the SEP responses of S1, S2, and S7 were very noisy. For S1 and S7, the responses were, firstly, diminished from NS to SL20 and then, a considerable amount increased from 20 to 30dB SL. Furthermore, For S5 and S6, the amplitudes were a little bit increased linearly. However, there were no clearly increased trends for S3, S4, and S7.

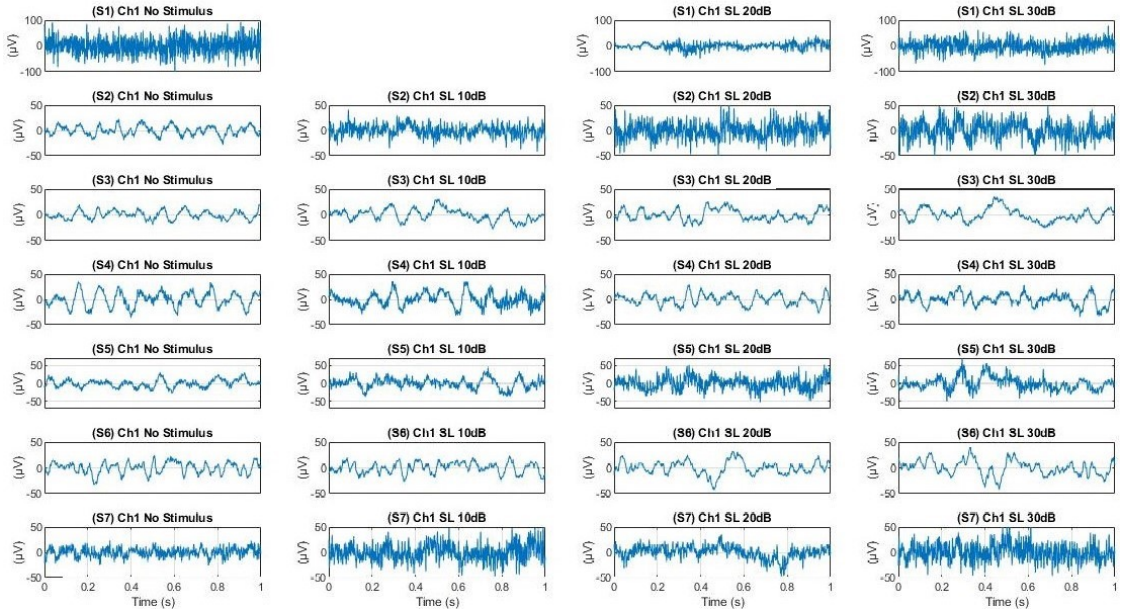

Figure 4.1 CH1 average data outputs of all subjects

According to Figure 4.2, compared to CH1 activities, only more minor changes were able to be observed, which generally have no meaning because it was considered as control channel. For S1 responses, there was a decrease from NS to 20dB SL, but then it increased from 20 to 30dB. For only the S2 subject, there could be seen a positive trend. For S3, S4, S5, S6, and S7 participants, any clear trends could not be observed because CH2 is the control channel as mentioned.

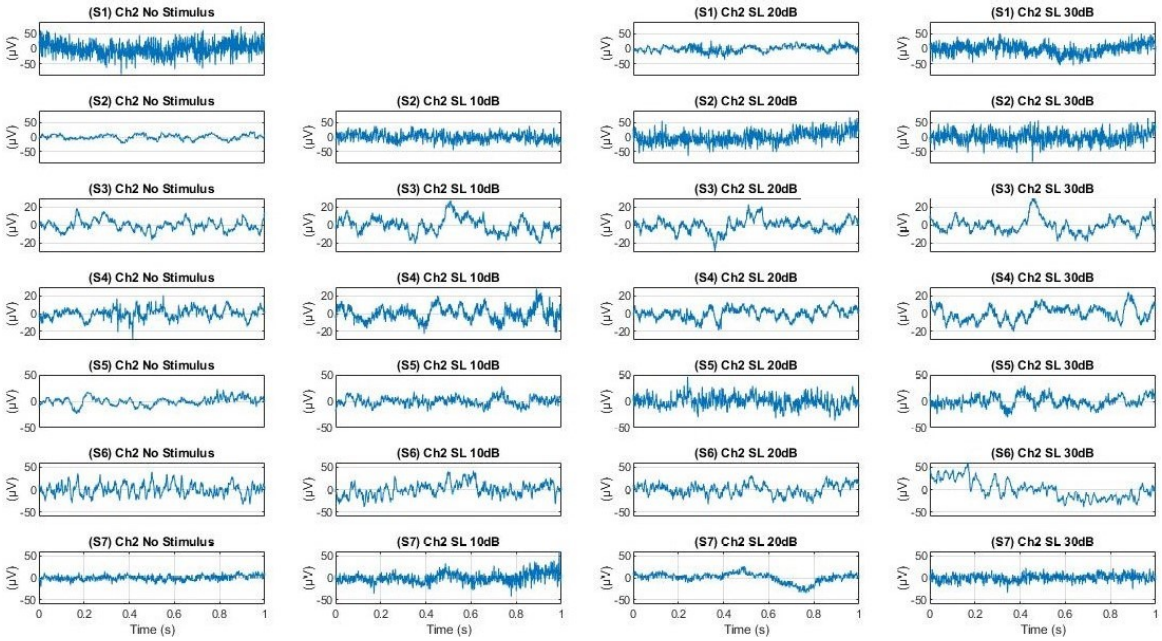

Figure 4.2 CH2 average data outputs of all subjects

4.2 Time-Frequency Plots and EEG Bands

Each raw SEP response was projected onto the frequency domain, and all CH1 signals were subtracted from CH2 ones with respect to the subject and SL based, then averaged them of all subjects for various SLs. After that, they monitored as average scalogram plot (Figure 4.3). In the plot, red areas represent the highest while the dark blue ones represent the lowest amplitudes. According to Figure 4.3, any periodic response could not be found for stimulus (40 Hz) frequency. Furthermore, as it can

be seen on the magnitude scalogram projection, for high-frequency levels (high gamma band), there was a little bit diminished trend in terms of magnitude from NS to 10dB SL. Afterward, there was a barely but visibly increase in magnitude from 10dB to 20 and 30dB SLs at the same frequency areas. However, any difference cannot be observed for other frequency bands depending on the SLs.

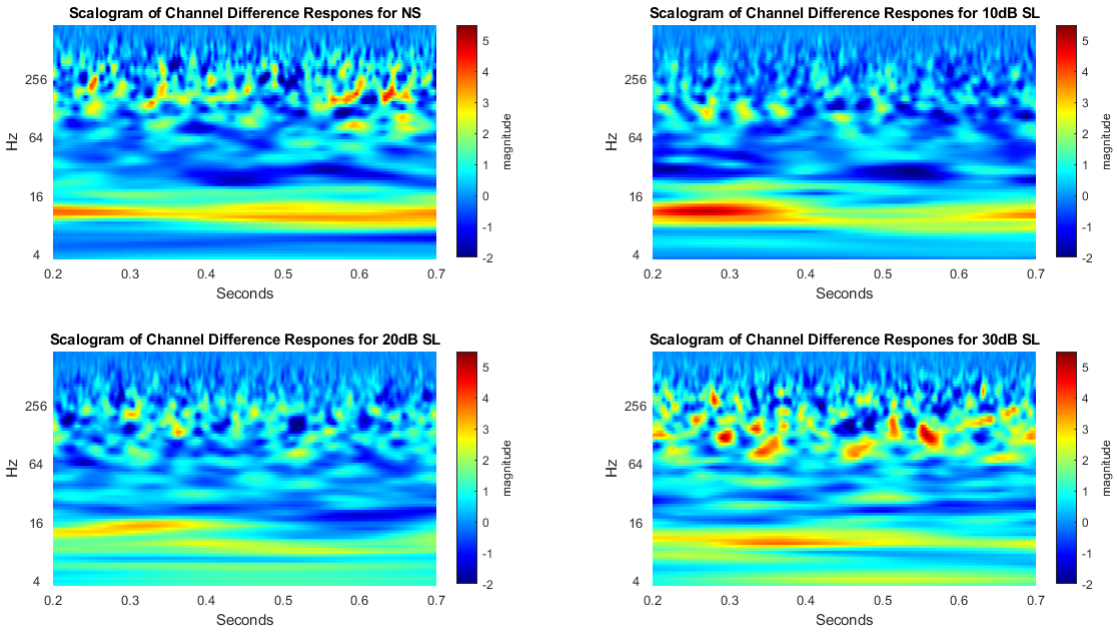

Figure 4.3 Scalogram Plots of CH1 and CH2 difference data for all SLs

The data were separated into two different (*Ro* represent 0.2-0.3s of the time course and *Rd** is 0.3-0.7s of the recording time) time windows (TWs), and it was averaged in time axis for both TWs, then it was plotted in order to show frequency domain spectrum and see whether there was a prominent peak or not during the stimulus (onset) period.

According to Figure 4.4, only 30dB SL visibly differ from other sensation levels (NS, 10, and 20dB) in terms of amplitudes at higher frequency levels (stimulus, low gamma, and high gamma bands) for *Rd**. However, any significant differences in peaks among SLs could not be shown for either around stimulus or other frequency bands (alpha-beta and wide-band).

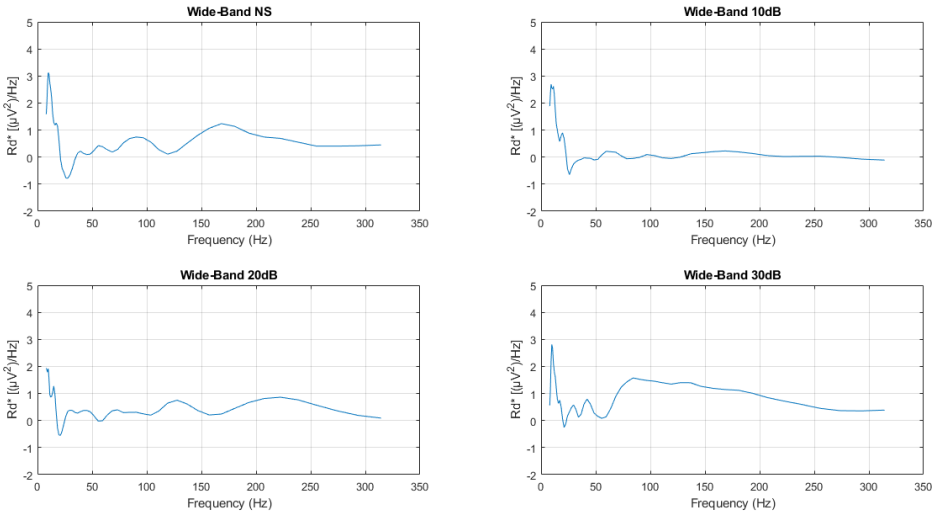

Figure 4.4 *Rd** Wide-Band frequency domain responses for all SLs

In Figure 4.5, *Ro* magnitude responses of wide-band were plotted. These plots did not show prominent peaks for low gamma, stimulus, and high gamma bands. On the other hand, likewise *Rd** TW, 30dB SL has higher amplitudes compared to other SLs, as well.

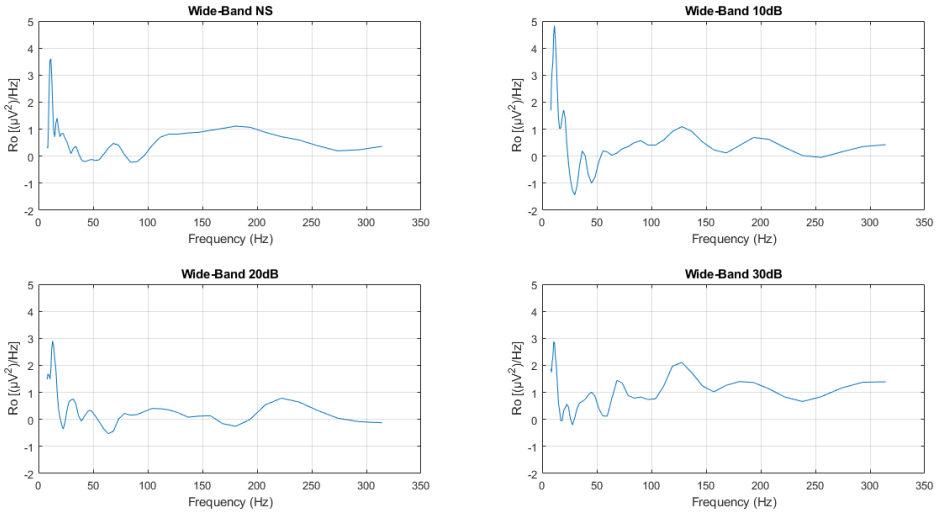

Figure 4.5 *Ro* Wide-Band frequency domain responses for all SLs

4.3 Average Magnitudes and Statistical Analysis

For sensation level, any significant differences were not able to be found. However, for overall Rd^* data, the factor of frequency band was found as significant with the p = 0.010 according to sphericity assumed value. Post-hoc test exhibited (Fisher′s Least Significant Differences in estimated marginal means) that alpha-beta, low gamma (p = 0.028) and stimulus band (p = 0.023) were significantly different, but there was not found a significant correlation between alpha-beta and wide-band. There was no significant difference between high gamma and resting (low gamma, stimulus band, and wide-band) frequency bands. Moreover, there was a statistically significant difference between low gamma and wide-band with the p-value of 0.030; however, there was no significant difference between low gamma and stimulus band, and stimulus band and wideband (Figure 4.6 and Table 4.1). Even more, observed power of this analysis was also very weak since observed power of SL and frequency band parameters were found as 0.131 and 0.420 respectively.

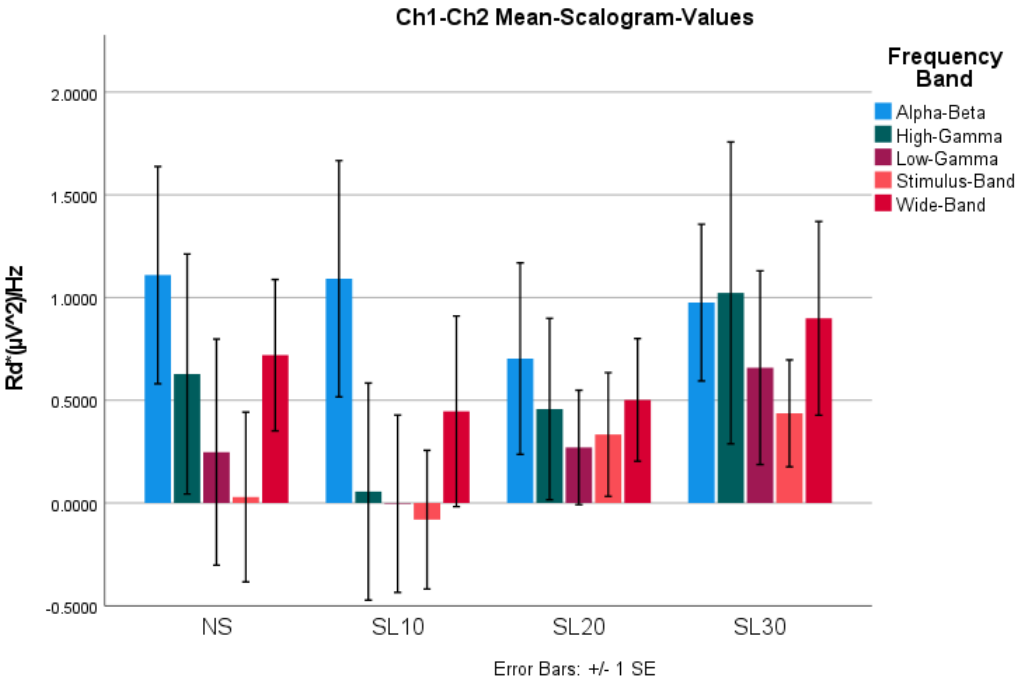

Figure 4.6 Amplitudes of channel difference data for Rd^* time window in the various frequency bands

Furthermore, for Rd^* NS, stimulus band and the wide-band was observed as

significant p = 0.004. Like NS, there was a statistically significant effect between stimulus band and wide-band with the p-value of 0.032 for 10dB SL, and also, stimulus band and alpha-beta were observed as significant (p = 0.026). However, for 20dB and 30dB SL, there were no significant main effects among EEG frequency bands (Table 4.2). Even more, as it can be seen on the Table 4.3, there is no effect of the frequency band energies on SL correlations.

For overall *Ro* data, SL was not significant likewise *Rd** data. Frequency band had a significant main effect (p = 0.006) corresponding to sphericity assumed values. According to post-hoc there was a statistically significant difference between alpha-beta and low gamma (p = 0.015), stimulus band (p = 0.016), wide-band (p = 0.047), but there was no difference between high gamma and remaining (low gamma, stimulus band, and wide-band) bands. A significant difference was found between low gamma and the wide-band (p = 0.012), but low gamma and stimulus band were not found as significant. Lastly, There was no significant difference between stimulus band and wide-band (Figure 4.7 and Table 4.1).

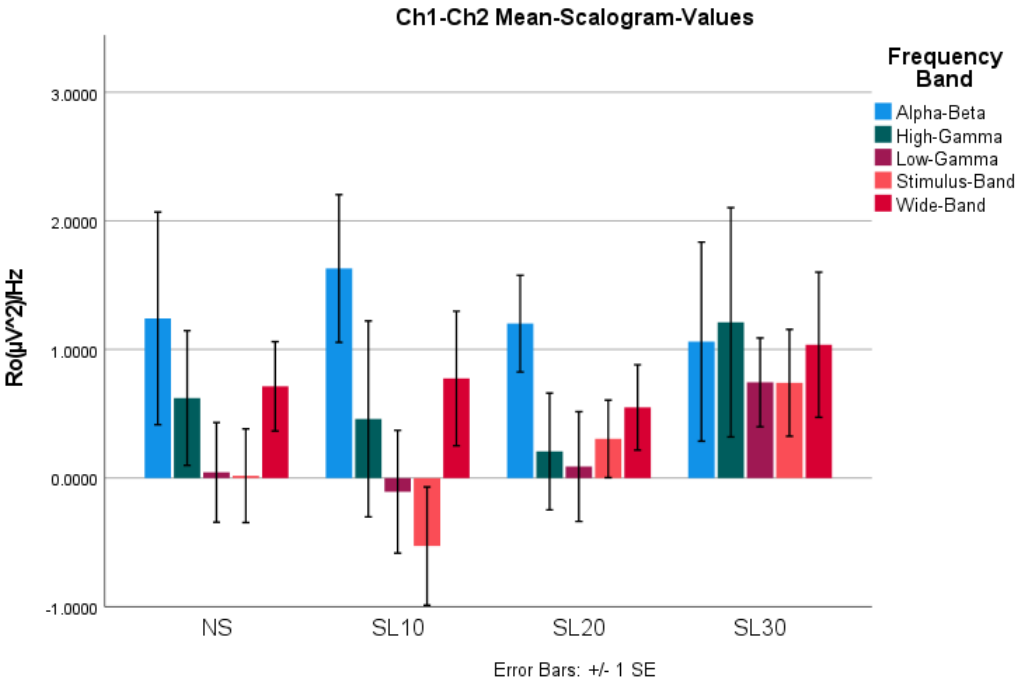

Figure 4.7 Amplitudes of channel difference data for *Ro* time window in the various frequency bands

Moreover, For NS *Ro* data, significant main effect was found between stimulus band and wide-band (p = 0.044) likewise Rd^*. For 10dB SL, there was a statistically significant effect between alpha-beta and low gamma (p = 0.009), stimulus band (p = 0.001). Wide-band and low gamma (p = 0.003), and stimulus band (p = 0.004) were observed as statistically significant. But, for 20dB and 30dB SL, any significant effect could not be found (Table 4.2).

Furthermore, for *Ro* low-gamma, there was a significant correlation between SL30 and NS (p = 0.025), SL20 (p = 0.023) (Table 4.3). However, statistical power of SL was found 0.11 and frequency band parameter was 0.165, which were very low, in Ro TW.

Table 4.1
Pairwise comparisons for various sensation levels and frequency bands for two TWs.

Analysis Parameter	Comparisons		*Ro*	Rd^*
Sensation Level	NS - 10dB SL	p	0.989	0.869
	NS - 20dB SL	p	0.988	0.467
	NS - 30dB SL	p	0.362	0.445
	10dB SL - 20dB SL	p	0.945	0.469
	10dB SL - 30dB SL	p	0.114	0.176
	20dB SL - 30dB SL	p	0.141	0.475
Frequency Band	Alpha-Beta - High Gamma	p	0.109	0.104
	Alpha-Beta - Low Gamma	p	0.015*	0.028*
	Alpha-Beta - Stimulus Band	p	0.016*	0.023*
	Alpha-Beta - Wide Band	p	0.047*	0.056
	High Gamma - Low Gamma	p	0.500	0.581
	High Gamma - Stimulus Band	p	0.637	0.750
	High Gamma - Wide Band	p	0.273	0.227
	Low Gamma - Stimulus Band	p	0.993	0.942
	Low Gamma - Wide Band	p	0.012*	0.030*
	Stimulus Band - Wide Band	p	0.084	0.131

Table 4.2
The effect of frequency band energies on correlations of sensation levels for two TWs.

Sensation Level	Frequency Band		*Ro*	*Rd**
NS	Alpha-Beta - High Gamma	p	0.611	0.614
	Alpha-Beta - Low Gamma	p	0.253	0.281
	Alpha-Beta - Stimulus Band	p	0.227	0.091
	Alpha-Beta - Wide Band	p	0.448	0.467
	High Gamma - Low Gamma	p	0.137	0.217
	High Gamma - Stimulus Band	p	0.107	0.227
	High Gamma - Wide Band	p	0.864	0.830
	Low Gamma - Stimulus Band	p	0.740	0.338
	Low Gamma - Wide Band	p	0.083	0.104
	Stimulus Band - Wide Band	p	0.044*	0.004*
10dB SL	Alpha-Beta - High Gamma	p	0.174	0.075
	Alpha-Beta - Low Gamma	p	0.009*	0.084
	Alpha-Beta - Stimulus Band	p	0.001*	0.026*
	Alpha-Beta - Wide Band	p	0.062	0.074
	High Gamma - Low Gamma	p	0.254	0.820
	High Gamma - Stimulus Band	p	0.169	0.659
	High Gamma - Wide Band	p	0.458	0.100
	Low Gamma - Stimulus Band	p	0.080	0.687
	Low Gamma - Wide Band	p	0.003*	0.125
	Stimulus Band - Wide Band	p	0.004*	0.032*
20dB SL	Alpha-Beta - High Gamma	p	0.089	0.708
	Alpha-Beta - Low Gamma	p	0.083	0.347
	Alpha-Beta - Stimulus Band	p	0.114	0.320
	Alpha-Beta - Wide Band	p	0.079	0.556
	High Gamma - Low Gamma	p	0.653	0.611
	High Gamma - Stimulus Band	p	0.811	0.820
	High Gamma - Wide Band	p	0.137	0.892
	Low Gamma - Stimulus Band	p	0.450	0.773
	Low Gamma - Wide Band	p	0.118	0.232
	Stimulus Band - Wide Band	p	0.462	0.551
30dB SL	Alpha-Beta - High Gamma	p	0.884	0.943
	Alpha-Beta - Low Gamma	p	0.636	0.491
	Alpha-Beta - Stimulus Band	p	0.717	0.161
	Alpha-Beta - Wide Band	p	0.960	0.821
	High Gamma - Low Gamma	p	0.540	0.292
	High Gamma - Stimulus Band	p	0.685	0.383
	High Gamma - Wide Band	p	0.764	0.703
	Low Gamma - Stimulus Band	p	0.993	0.530
	Low Gamma - Wide Band	p	0.418	0.180
	Stimulus Band - Wide Band	p	0.694	0.244

Table 4.3
The effect of SLs on correlations of frequency band energies for two TWs.

Frequency Band	Sensation Level		*Ro*	*Rd**
Alpha-Beta	NS - 10dB SL	p	0.989	0.329
	NS - 20dB SL	p	0.736	0.137
	NS - 30dB SL	p	0.761	0.721
	10dB SL - 20dB SL	p	0.449	0.699
	10dB SL - 30dB SL	p	0.584	0.929
	20dB SL - 30dB SL	p	0.923	0.726
High Gamma	NS - 10dB SL	p	0.614	0.928
	NS - 20dB SL	p	0.751	0.580
	NS - 30dB SL	p	0.470	0.342
	10dB SL - 20dB SL	p	0.351	0.531
	10dB SL - 30dB SL	p	0.559	0.100
	20dB SL - 30dB SL	p	0.148	0.297
Low Gamma	NS - 10dB SL	p	0.974	0.734
	NS - 20dB SL	p	0.698	0.266
	NS - 30dB SL	p	0.025*	0.149
	10dB SL - 20dB SL	p	0.608	0.370
	10dB SL - 30dB SL	p	0.058	0.128
	20dB SL - 30dB SL	p	0.023*	0.468
Stimulus Band	NS - 10dB SL	p	0.319	0.857
	NS - 20dB SL	p	0.200	0.095
	NS - 30dB SL	p	0.074	0.209
	10dB SL - 20dB SL	p	0.149	0.080
	10dB SL - 30dB SL	p	0.116	0.126
	20dB SL - 30dB SL	p	0.219	0.194
Wide-Band	NS - 10dB SL	p	0.828	0.755
	NS - 20dB SL	p	0.769	0.855
	NS - 30dB SL	p	0.738	0.593
	10dB SL - 20dB SL	p	0.180	0.802
	10dB SL - 30dB SL	p	0.695	0.273
	20dB SL - 30dB SL	p	0.334	0.429

5. DISCUSSION

In this thesis, the influence of 40 Hz vibrotactile stimulation on human EEG over the somatosensory cortex was observed. For observations, The stimulus parameter (SLs), onset and remaining time (TWs), and frequency band were considered. In order to verify this, extracted CH1 brain responses were subtracted from CH2 ones and then were analyzed by TFA. After that, the time-frequency information was averaged for specific regions either in the time or frequency domain for seven subjects for each stimulus level.

For scalogram (Figure 4.3) and frequency domain plots (Figure 4.4 and Figure 4.5), clear peaks or periodic patterns were not able to be observed, unlike responses in mechanoreceptive fibers and cortical neurons, which may be related to the characteristic feature of RA like fibers, periodic firings are not produced by P neurons in the S1 cortex at the low stimulus level [93, 94]. Likewise pointed out in the literature, those time-frequency figures and power plots could not show such precise results for lower stimulus intensities. On the contrary, robust spike activities can be recorded from mechanoreceptive fibers and cortical neurons at these low stimulus levels. However, when the magnitudes were averaged and statistically analyzed, SL30 and NS were, parametrically, found as significant for only *Ro* low-gamma, but other ones were not significant, which displays that the relationship between stimulus intensity and activation could not be established in this EEG data.

Even more, the frequency band parameter was analytically observed as significant (Figure 4.6 and Figure 4.7). These analyses were not done in previous works that are related to this experiment [95, 8]. For both Rd^* and *Ro* data, significant activities were observed between alpha-beta and low gamma, alpha-beta and stimulus band, low gamma and wide-band. However, any significant correlation was not observed for other frequency bands. In other words, the stimulus band (32-48 Hz) and low gamma (32-90 Hz), which also covers the stimulus band, bands may differ from other frequency bands

during the whole stimulus period (0.2-0.7s) since there was no significant correlation between TWs (Rd^* and Ro). Furthermore, retrospectively on human experiments, it was shown that S1 activity was directly modulated with attention, and by the attention, it may be significantly enhanced [96, 97, 98, 99, 100]. It was mentioned that concentration or attention led to gamma activities [101]. In our experiments, subjects may extremely focused on the experiment, so this may be another reason why the low gamma-band activity was significant.

The average data of 7 subjects in each stimulus level was much more unclear, so the overall effect of SL could not be shown. However, for SL10 dB in both Rd^* and Ro, there were somewhat more significantly correlated frequency bands compared to NS, but this was not observed for other SLs (SL20 and SL30 dB). It can partially be deducted that although SL has no significant main effect, more frequency differences can be observed to some extent. It means that if the stimulus intensity is slightly increased, such as from NS to 10dB, more frequency bands could be found as significant. Furthermore, as it was, previously, mentioned, SL30 and NS were significant for Ro low-gamma band. It can be asserted that there can be an influence of the presence of their intensity adequately high or the absence of the stimulus on frequency parameters to study somatosensory processing. This result is similar to previous studies in literature, as well [95, 8, 15].

6. CONCLUSIONS

In this thesis, SL, TW, and frequency band parameters were observed to determine if there were an influence on EEG over the S1 cortex for 40 Hz vibrotactile stimulus with non-invasive recording methods, and they were substantial criteria in somatosensory processing and psychophysical experiments. According to findings, SL and TW had no overall effect on this EEG. The influence of the SL was shown only in a certain type of frequency band (for low gamma) and TW (for *Ro*), which may suggest that neural activity may increase at the onset of vibrotactile stimulation. Overall, this particular experimental data could not distinguish psychophysical parameters by the presented methods.

7. LIMITATIONS

Most of the subjects were university students in the research, so it does not comprise the whole population. Since the tactile sensitivity diminished corresponding to age, participants were selected within a narrow (22-29) range in terms of age. Very few amounts of subjects were participated, which may be related to the long duration of the experiments.

Finding electrode location was somewhat difficult on every subject, which may negatively influence the collected data. Furthermore, during experiments, subjects were moved due to missing comfort, which resulted in artifacts of motion. Although the procedure was conducted in an isolated environment, there were still much more noises for some subjects′ recordings. Even more, each signal was averaged 100 times, yet still, the background noises could not be reduced sufficiently, which implicates that non-invasive recording methods cannot be a good way to observe psychophysical parameters. The solution to this may be to extract these data by invasive (e.g. ECoG) recordings.

Furthermore, observing single-trial activity can sometimes be important, but the experimental setup automatically averaged the data, so they were not collected as trial-by-trial, which restricts us from analyzing and observing the trial-by-trial activity since some recordings were noisy, and this was also not feasible.

REFERENCES

1. Kandel, E. R., J. H. Schwartz, T. M. Jessell, S. Siegelbaum, A. J. Hudspeth, and S. Mack, *Principles of neural science*, Vol. 4, McGraw-hill New York, 2000.

2. Kim, D. J., J. Ying, and J. Shen, "Regulation of the inflammatory process in osteoarthritis," 2020.

3. Benmoussa, S., R. Merzouki, and B. O. Bouamama, "Bond graph model-based fault detection and isolation: Application to intelligent autonomous vehicles," *Mechatronic & Innovative Applications*, p. 111, 2012.

4. Bear, M. F., B. W. Connors, and M. A. Paradiso, *Neuroscience: exploring the brain*, Baltimore, Md: Lippincott Williams & Wilkins, 2nd ed ed., 2001.

5. Welker, W. I., J. I. Johnson, and B. H. Pubols, "SOME MORPHOLOGICAL AND PHYSIOLOGICAL CHARACTERISTICS OF THE SOMATIC SENSORY SYSTEM IN RACCOONS," *American Zoologist*, Vol. 4, pp. 75–94, Feb. 1964.

6. Greenspan, J. D., and S. J. Bolanowski, "The psychophysics of tactile perception and its peripheral physiological basis," in *Pain and touch*, pp. 25–103, Elsevier, 1996.

7. Bear, M. F., B. W. Connors, and M. A. Paradiso, *Neuroscience: exploring the brain*, Philadelphia, PA: Lippincott Williams & Wilkins, 3rd ed ed., 2007. OCLC: ocm62509134.

8. YILDIZ, M. Z., *EFFECTS OF MECHANICAL AND TEMPORAL PARAMETERS ON TACTILE PSYCHOPHYSICAL RESPONSES*. PhD thesis, Institute of Biomedical Engineering, 2013.

9. Gibson, J. J., "Observations on active touch.," *Psychological review*, Vol. 69, no. 6, p. 477, 1962.

10. Schaefer, U. F., S. Hansen, M. Schneider, J. L. Contreras, and C.-M. Lehr, "Models for skin absorption and skin toxicity testing," in *Drug absorption studies*, pp. 3–33, Springer, 2008.

11. Bear, M., B. Connors, and M. A. Paradiso, *Neuroscience: Exploring the brain*, Jones & Bartlett Learning, LLC, 2020.

12. Hendriks, F. M., "Mechanical behaviour of human epidermal and dermal layers in vivo.," 2005.

13. Johansson, R. S., and Ã. B. Vallbo, "Tactile sensory coding in the glabrous skin of the human hand," *Trends in Neurosciences*, Vol. 6, pp. 27–32, Jan. 1983.

14. Güçlü, B., and S. J. Bolanowski, "Distribution of the intensity-characteristic parameters of cat rapidly adapting mechanoreceptive fibers," *Somatosensory & motor research*, Vol. 20, no. 2, pp. 149–155, 2003.

15. Güçlü, B., and S. J. Bolanowski, "Frequency responses of cat rapidly adapting mechanoreceptive fibers," *Somatosensory & motor research*, Vol. 20, no. 3-4, pp. 249–263, 2003.

16. Güçlü, B., and S. J. Bolanowski, "Tristate markov model for the firing statistics of rapidly-adapting mechanoreceptive fibers," *Journal of computational neuroscience*, Vol. 17, no. 2, pp. 107–126, 2004.

17. Güçlü, B., and S. J. Bolanowski, "Modeling population responses of rapidly-adapting mechanoreceptive fibers," *Journal of Computational Neuroscience*, Vol. 12, no. 3, pp. 201–218, 2002.

18. Güçlü, B., and S. J. Bolanowski, "Probability of stimulus detection in a model population of rapidly adapting fibers," *Neural computation*, Vol. 16, no. 1, pp. 39–58, 2004.

19. Bolanowski Jr, S. J., G. A. Gescheider, R. T. Verrillo, and C. M. Checkosky, "Four channels mediate the mechanical aspects of touch," *The Journal of the Acoustical society of America*, Vol. 84, no. 5, pp. 1680–1694, 1988.

20. Mountcastle, V. B., R. H. LaMotte, and G. Carli, "Detection thresholds for stimuli in humans and monkeys: comparison with threshold events in mechanoreceptive afferent nerve fibers innervating the monkey hand.," *Journal of Neurophysiology*, Vol. 35, no. 1, pp. 122–136, 1972.

21. Samuels, M. A., S. K. Feske, and K. R. Daffner, *Office practice of neurology*, Gulf Professional Publishing, 2003.

22. Mountcastle, V. B., "The columnar organization of the neocortex.," *Brain: a journal of neurology*, Vol. 120, no. 4, pp. 701–722, 1997.

23. Kaas, J., R. Nelson, M. Sur, and M. Merzenich, "Organization of somatosensory cortex in primates," in *The organization of the cerebral cortex*, pp. 237–261, MIT Press Cambridge, MA, 1981.

24. Sur, M., J. T. Wall, and J. Kaas, "Modular distribution of neurons with slowly adapting and rapidly adapting responses in area 3b of somatosensory cortex in monkeys," *Journal of neurophysiology*, Vol. 51, no. 4, pp. 724–744, 1984.

25. Dudel, J., "General sensory physiology," in *Human Physiology*, pp. 177–192, Springer, 1983.

26. Gescheider, G. A., *Psychophysics: the fundamentals*, Mahwah, N.J: L. Erlbaum Associates, 3rd ed ed., 1997.

27. Zwislocki, J. J., and E. M. Relkin, "On a psychophysical transformed-rule up and down method converging on a 75% level of correct responses," *Proceedings of the National Academy of Sciences*, Vol. 98, no. 8, pp. 4811–4814, 2001.

28. Gescheider, G. A., S. J. Bolanowski, and R. T. Verrillo, "Some characteristics of tactile channels," *Behavioural brain research*, Vol. 148, no. 1-2, pp. 35–40, 2004.

29. Gescheider, A., S. J. Bolanowski, and K. R. Hardick, "The frequency selectivity of information-processing channels in the tactile sensory system," *Somatosensory & Motor Research*, Vol. 18, no. 3, pp. 191–201, 2001.

30. Gescheider, G. A., S. J. Bolanowski, J. V. Pope, and R. T. Verrillo, "A four-channel analysis of the tactile sensitivity of the fingertip: frequency selectivity, spatial summation, and temporal summation," *Somatosensory & motor research*, Vol. 19, no. 2, pp. 114–124, 2002.

31. Bolanowski Jr, S., and J. J. Zwislocki, "Intensity and frequency characteristics of pacinian corpuscles. i. action potentials," *Journal of neurophysiology*, Vol. 51, no. 4, pp. 793–811, 1984.

32. Gescheider, G. A., R. T. Verrillo, and C. L. Van Doren, "Prediction of vibrotactile masking functions," *The Journal of the Acoustical Society of America*, Vol. 72, no. 5, pp. 1421–1426, 1982.

33. Brain, W. R., R. Bannister, *et al.*, *Brain's clinical neurology*, Oxford University Press, 1985.

34. Kass, J. S., and E. M. Mizrahi, *Neurology secrets e-book*, Elsevier Health Sciences, 2010.

35. Boutros, N. N., and A. Belger, "Midlatency evoked potentials attenuation and augmentation reflect different aspects of sensory gating," *Biological psychiatry*, Vol. 45, no. 7, pp. 917–922, 1999.

36. Allison, T., G. McCarthy, and C. C. Wood, "The relationship between human long-latency somatosensory evoked potentials recorded from the cortical surface and from the scalp," *Electroencephalography and Clinical Neurophysiology/Evoked Potentials Section*, Vol. 84, no. 4, pp. 301–314, 1992.

37. Misulis, K. E., "Spehlmann's evoked potential primer," *Visual, auditory and somatosensory evoked potentials in clinical diagnosis*, 1994.

38. Zouridakis, G., "Contributions of technological developments to imaging," in *Biomedical Technology and Devices Handbook*, pp. 217–218, CRC Press, 2003.

39. Hoppe, U., K. Schnabel, S. Weiss, and I. Rundshagen, "Representation of somatosensory evoked potentials using discrete wavelet transform," *Journal of clinical monitoring and computing*, Vol. 17, no. 3, pp. 227–233, 2002.

40. Caruso, G., M. Nolano, F. Lullo, C. Crisci, J. B. Nilsson, and R. Massini, "Median nerve sensory responses evoked by tactile stimulation of the finger proximal and distal phalanx in normal subjects," *Muscle & Nerve: Official Journal of the American Association of Electrodiagnostic Medicine*, Vol. 17, no. 3, pp. 269–275, 1994.

41. Kelly, E. F., M. Trulsson, and S. E. Folger, "Periodic microstimulation of single mechanoreceptive afferents produces frequency-following responses in human eeg," *Journal of neurophysiology*, Vol. 77, no. 1, pp. 137–144, 1997.

42. Kelly, E. F., and S. E. Folger, "Eeg evidence of stimulus-directed response dynamics in human somatosensory cortex," *Brain research*, Vol. 815, no. 2, pp. 326–336, 1999.

43. Yoo, S.-J., S. Ryu, S. Kim, H. S. Han, C. Moon, *et al.*, "Reference module in neuroscience and biobehavioral psychology," 2017.

44. Van Drongelen, W., *Signal processing for neuroscientists: an introduction to the analysis of physiological signals*, Academic press, 2018.

45. Abhang, P. A., B. W. Gawali, and S. C. Mehrotra, *Introduction to EEG-and speech-based emotion recognition*, Academic Press, 2016.

46. Abhang, P. A., B. W. Gawali, and S. C. Mehrotra, "Technological basics of eeg recording and operation of apparatus," in *Introduction to EEG-and Speech-Based Emotion Recognition*, pp. p19–p50, Academic Press, 2016.

47. Kojima, S., N. Otsuru, S. Miyaguchi, H. Yokota, K. Nagasaka, K. Saito, Y. Inukai, H. Shirozu, and H. Onishi, "The intervention of mechanical tactile stimulation modulates somatosensory evoked magnetic fields and cortical oscillations," *European Journal of Neuroscience*, 2021.

48. Li, W., C. Li, Q. Xu, and L. Ji, "Effects of focal vibration over upper limb muscles on the activation of sensorimotor cortex network: an eeg study," *Journal of healthcare engineering*, Vol. 2019, 2019.

49. Lopez, S., F. Bini, C. Del Percio, F. Marinozzi, C. Celletti, A. Suppa, R. Ferri, E. Staltari, F. Camerota, and C. Babiloni, "Electroencephalographic sensorimotor rhythms are modulated in the acute phase following focal vibration in healthy subjects," *Neuroscience*, Vol. 352, pp. 236–248, 2017.

50. Narayan, R., *Encyclopedia of biomedical engineering*, Elsevier, 2018.

51. Molla, M. K. I., S. Das, M. E. Hamid, and K. Hirose, "Empirical mode decomposition for advanced speech signal processing," *Journal of Signal Processing*, Vol. 17, no. 6, pp. 215–229, 2013.

52. Altamirano, A. A., *EMG pattern prediction for upper limb movements based on wavelet and Hilbert-Huang transform.* PhD thesis, Université de Lorraine; Instituto politécnico nacional (México), 2017.

53. Huang, N. E., Z. Shen, S. R. Long, M. C. Wu, H. H. Shih, Q. Zheng, N.-C. Yen, C. C. Tung, and H. H. Liu, "The empirical mode decomposition and the hilbert spectrum for nonlinear and non-stationary time series analysis," *Proceedings of the Royal Society of London. Series A: mathematical, physical and engineering sciences*, Vol. 454, no. 1971, pp. 903–995, 1998.

54. Perraudin, N., B. Ricaud, D. I. Shuman, and P. Vandergheynst, "Global and local uncertainty principles for signals on graphs," *APSIPA Transactions on Signal and Information Processing*, Vol. 7, 2018.

55. Klonowski, W., "Everything you wanted to ask about eeg but were afraid to get the right answer," *Nonlinear biomedical physics*, Vol. 3, no. 1, pp. 1–5, 2009.

56. Cohen, M. X., *MATLAB for brain and cognitive scientists*, MIT Press, 2017.

57. Cohen, M. X., *Analyzing neural time series data: theory and practice*, MIT press, 2014.

58. Mouraux, A., and G. D. Iannetti, "Across-trial averaging of event-related eeg responses and beyond," *Magnetic resonance imaging*, Vol. 26, no. 7, pp. 1041–1054, 2008.

59. "Time-frequency gallery." https://www.mathworks.com/help/wavelet/ug/time-frequency-gallery.html, 2021.

60. Wang, P., J. Gao, and Z. Wang, "Time-frequency analysis of seismic data using synchrosqueezing transform," *IEEE Geoscience and Remote Sensing Letters*, Vol. 11, no. 12, pp. 2042–2044, 2014.

61. Zhao, Y., H. Cui, H. Huo, and Y. Nie, "Application of synchrosqueezed wavelet transforms for extraction of the oscillatory parameters of subsynchronous oscillation in power systems," *Energies*, Vol. 11, no. 6, p. 1525, 2018.

62. Moody, G. B., and R. G. Mark, "The impact of the mit-bih arrhythmia database," *IEEE Engineering in Medicine and Biology Magazine*, Vol. 20, no. 3, pp. 45–50, 2001.

63. Lashermes, B., E. Foufoula-Georgiou, and W. E. Dietrich, "Channel network extraction from high resolution topography using wavelets," *Geophysical Research Letters*, Vol. 34, no. 23, 2007.

64. Doglioni, A., and V. Simeone, "Quantitative geomorphological analysis based on wavelet transforms," in *Landslide science and practice*, pp. 257–264, Springer, 2013.

65. Ferretti, A., C. Prati, and F. Rocca, "Multibaseline insar dem reconstruction: The wavelet approach," *IEEE Transactions on geoscience and remote sensing*, Vol. 37, no. 2, pp. 705–715, 1999.

66. Unser, M., and A. Aldroubi, "A review of wavelets in biomedical applications," *Proceedings of the IEEE*, Vol. 84, no. 4, pp. 626–638, 1996.

67. Tse, N. C., and L. Lai, "Wavelet-based algorithm for signal analysis," *EURASIP Journal on Advances in Signal Processing*, Vol. 2007, pp. 1–10, 2007.

68. Percival, D., and A. Walden, "continuous and discrete wavelet transforms (cambridge up, cambridge, uk)," 2000.

69. "Practical introduction to continuous analysis." https://www.mathworks.com/help/wavelet/ug/practical-introduction-to-continuous-analysis.html, 2021.

70. Percival, D., and A. Walden, "Wavelet methods for time series analysis (cambridge up, cambridge, uk)," 2000.

71. Shen, Y., and V. Giurgiutiu, "Predictive modeling of nonlinear wave propagation for structural health monitoring with piezoelectric wafer active sensors," *Journal of Intelligent Material Systems and Structures*, Vol. 25, no. 4, pp. 506–520, 2014.

72. Grossmann, A., and J. Morlet, "Decomposition of hardy functions into square integrable wavelets of constant shape," *SIAM journal on mathematical analysis*, Vol. 15, no. 4, pp. 723–736, 1984.

73. Olhede, S. C., and A. T. Walden, "Generalized morse wavelets," *IEEE Transactions on Signal Processing*, Vol. 50, no. 11, pp. 2661–2670, 2002.

74. Daubechies, I., *Ten lectures on wavelets*, SIAM, 1992.

75. "Signal multiresolution analyzer." https://www. mathworks. com/help/wavelet/gs/choose-a-wavelet.html, 2021.

76. Silik, A., M. Noori, W. A. Altabey, R. Ghiasi, and Z. Wu, "Comparative analysis of wavelet transform for time-frequency analysis and transient localization in structural health monitoring," *Structural Durability & Health Monitoring*, Vol. 15, no. 1, p. 1, 2021.

77. Fabrizi, L., G. Williams, A. Lee, J. Meek, R. Slater, S. Olhede, and M. Fitzgerald, "Cortical activity evoked by an acute painful tissue-damaging stimulus in healthy adult volunteers," *Journal of neurophysiology*, Vol. 109, no. 9, pp. 2393–2403, 2013.

78. Burgess, A. P., "How conventional visual representations of time-frequency analyses bias our perception of eeg/meg signals and what to do about it," *Frontiers in human neuroscience*, Vol. 13, p. 212, 2019.

79. Leicht, G., V. Kirsch, I. Giegling, S. Karch, I. Hantschk, H.-J. Möller, O. Pogarell, U. Hegerl, D. Rujescu, and C. Mulert, "Reduced early auditory evoked gamma-band response in patients with schizophrenia," *Biological psychiatry*, Vol. 67, no. 3, pp. 224–231, 2010.

80. Roach, B. J., and D. H. Mathalon, "Event-related eeg time-frequency analysis: an overview of measures and an analysis of early gamma band phase locking in schizophrenia," *Schizophrenia bulletin*, Vol. 34, no. 5, pp. 907–926, 2008.

81. van Driel, J., K. R. Ridderinkhof, and M. X. Cohen, "Not all errors are alike: theta and alpha eeg dynamics relate to differences in error-processing dynamics," *Journal of Neuroscience*, Vol. 32, no. 47, pp. 16795–16806, 2012.

82. Crewther, D. P., A. Brown, and L. Hugrass, "Temporal structure of human magnetic evoked fields," *Experimental brain research*, Vol. 234, no. 7, pp. 1987–1995, 2016.

83. Cohen, M. X., "A better way to define and describe morlet wavelets for time-frequency analysis," *NeuroImage*, Vol. 199, pp. 81–86, 2019.

84. Ortiz-Echeverri, C. J., S. Salazar-Colores, J. Rodríguez-Reséndiz, and R. A. Gómez-Loenzo, "A new approach for motor imagery classification based on sorted blind source separation, continuous wavelet transform, and convolutional neural network," *Sensors*, Vol. 19, no. 20, p. 4541, 2019.

85. Nakhnikian, A., S. Ito, L. Dwiel, L. Grasse, G. Rebec, L. Lauridsen, and J. Beggs, "A novel cross-frequency coupling detection method using the generalized morse wavelets," *Journal of neuroscience methods*, Vol. 269, pp. 61–73, 2016.

86. Lilly, J. M., and S. C. Olhede, "Higher-order properties of analytic wavelets," *IEEE Transactions on Signal Processing*, Vol. 57, no. 1, pp. 146–160, 2008.

87. Lilly, J. M., and S. C. Olhede, "On the analytic wavelet transform," *IEEE transactions on information theory*, Vol. 56, no. 8, pp. 4135–4156, 2010.

88. Lilly, J. M., and S. C. Olhede, "Generalized morse wavelets as a superfamily of analytic wavelets," *IEEE Transactions on Signal Processing*, Vol. 60, no. 11, pp. 6036–6041, 2012.

89. Lilly, J., "jlab. a data analysis package for matlab, v. 1.6. 2. 2016," *URL http://www. jmlilly. net/jmlsoft. html*, 2016.

90. "Effect of parameter values on morse wavelet shape." https://www.mathworks.com/help/wavelet/ug/morse-wavelets.html, 2021.

91. Güçlü, B., and S. J. Bolanowski, "Vibrotactile thresholds of the non-pacinian i channel: I. methodological issues," *Somatosensory & motor research*, Vol. 22, no. 1-2, pp. 49–56, 2005.

92. "Cwt filter bank." https://www.mathworks.com/help/wavelet/ref/cwtfilterbank.html, 2021.

93. Mountcastle, V. B., W. H. Talbot, H. Sakata, and J. Hyvärinen, "Cortical neuronal mechanisms in flutter-vibration studied in unanesthetized monkeys. neuronal periodicity and frequency discrimination.," *Journal of neurophysiology*, Vol. 32, no. 3, pp. 452–484, 1969.

94. Ferrington, D., and M. Rowe, "Differential contributions to coding of cutaneous vibratory information by cortical somatosensory areas i and ii," *Journal of Neurophysiology*, Vol. 43, no. 2, pp. 310–331, 1980.

95. Torun, D., M. Yildiz, and B. Guclu, "Frequency following brain oscillations evoked by vibrotactile stimulation of the distal phalanx in normal subjects," in *2009 14th National Biomedical Engineering Meeting*, pp. 1–5, IEEE, 2009.

96. Iguchi, Y., Y. Hoshi, M. Nemoto, M. Taira, and I. Hashimoto, "Co-activation of the secondary somatosensory and auditory cortices facilitates frequency discrimination of vibrotactile stimuli," *Neuroscience*, Vol. 148, no. 2, pp. 461–472, 2007.

97. Burton, H., N. Abend, A.-M. MacLeod, R. Sinclair, A. Snyder, and M. Raichle, "Tactile attention tasks enhance activation in somatosensory regions of parietal cortex: a positron emission tomography study," *Cerebral Cortex*, Vol. 9, no. 7, pp. 662–674, 1999.

98. Johansen-Berg, H., V. Christensen, M. Woolrich, and P. M. Matthews, "Attention to touch modulates activity in both primary and secondary somatosensory areas," *Neuroreport*, Vol. 11, no. 6, pp. 1237–1241, 2000.

99. Staines, W. R., S. J. Graham, S. E. Black, and W. E. McIlroy, "Task-relevant modulation of contralateral and ipsilateral primary somatosensory cortex and the role of a prefrontal-cortical sensory gating system," *Neuroimage*, Vol. 15, no. 1, pp. 190–199, 2002.

100. Schaefer, M., H.-J. Heinze, and M. Rotte, "Task-relevant modulation of primary somatosensory cortex suggests a prefrontal–cortical sensory gating system," *Neuroimage*, Vol. 27, no. 1, pp. 130–135, 2005.

101. Magazzini, L., and K. D. Singh, "Spatial attention modulates visual gamma oscillations across the human ventral stream," *Neuroimage*, Vol. 166, pp. 219–229, 2018.

102. Pandey, P., and K. Seeja, "Subject independent emotion recognition system for people with facial deformity: an eeg based approach," *Journal of Ambient Intelligence and Humanized Computing*, Vol. 12, no. 2, pp. 2311–2320, 2021.

103. Talbot, W. H., I. Darian-Smith, H. H. Kornhuber, and V. B. Mountcastle, "The sense of flutter-vibration: comparison of the human capacity with response patterns of mechanoreceptive afferents from the monkey hand.," *Journal of neurophysiology*, Vol. 31, no. 2, pp. 301–334, 1968.